NASA CR-135288
CMU-NASA-8

THE EFFECT OF MICROSTRUCTURE AND STRENGTH ON THE FRACTURE TOUGHNESS OF AN 18 Ni, 300 GRADE MARAGING STEEL

by J. A. Psioda and J. R. Low, Jr.

CARNEGIE-MELLON UNIVERSITY

prepared for

NATIONAL AERONAUTICS AND SPACE ADMINISTRATION

NASA Lewis Research Center
Contract NGR 39-087-003

FINAL REPORT

November 1977

1. Report No.	2. Government Accession No.	3. Recipient's Catalog No.
NASA CR 135288		

4. Title and Subtitle	5. Report Date
The Effect of Microstructure and Strength on the Fracture Toughness of an 18 Ni, 300 Grade Maraging Steel	November 1977-Final Report
	6. Performing Organization Code

7. Author(s)	8. Performing Organization Report No.
J. A. Psioda and J. R. Low, Jr.	NASA - 8
	10. Work Unit No.

9. Performing Organization Name and Address	11. Contract or Grant No.
Carnegie-Mellon University Department of Metallurgy & Materials Science 5000 Forbes Avenue Pittsburgh, Pennsylvania 15213	NGR-39-087-003
	13. Type of Report and Period Covered
12. Sponsoring Agency Name and Address	Grant
National Aeronautics and Space Administration Washington, D. C.	14. Sponsoring Agency Code

15. Supplementary Notes

Project Manager, William D. Klopp, Head, Materials Development Section, NASA Lewis Research Center, Cleveland, Ohio

16. Abstract

Fractography and metallographic sectioning were used to investigate the influence of microstructure and strength on the fracture toughness (K_{Ic}) and fracture mechanism of an 18 Ni, 300 grade maraging steel. Increased yield strength from 1442 to 2070 MN/m^2 through precipitation hardening results in a K_{Ic} loss from 143 to 55 $MN/m^{3/2}$. Ti (C, N) Ti_2S, and TiC inclusions in sizes from 1 to 8, 1 to 15, and 0.1 to 2 microns respectively serve as sites for void nucleation and lead to fracture by the dimpled rupture process in all strength levels considered. TiC nucleated dimples occupy more than half the fracture in all conditions. Void nucleation rate and resultant number of dimples per unit area of fracture increase with increasing yield strength. Average dimple size decreases with increasing strength and/or overaging which follows from the decreasing amount of stable void growth measured by sectioning tensile specimens. Ti(C, N) and Ti_2S inclusions fail by a combination of particle cleavage and particle matrix interface decohesion suggesting a critical stress plus plastic strain or energy criterion for failure. Void growth is assisted by crack branching along a path of TiC inclusions. Coalescence occurs in the highest strength materials by a combination of TiC void nucleation and premature separation at strengthening precipitates.

17. Key Words (Suggested by Author(s))	18. Distribution Statement
dimpled rupture, microstructure, fracture, fractography, void initiation, void growth, void coalescence	Unclassified - unlimited

19. Security Classif. (of this report)	20. Security Classif. (of this page)	21. No. of Pages	22. Price*
Unclassified	Unclassified		

* For sale by the National Technical Information Service, Springfield, Virginia 22151

INTRODUCTION

Considerable emphasis in the past decade or so has been placed on the development of structural metals having high strength-to-density ratios. Current and developing aerospace and pressure vessel technologies have imposed rather stringent requirements on structures and have necessitated the utilization of materials having a balance of fracture toughness and strength properties. In the attempt to maximize strength and satisfy the unusually high toughness requirements of today's designs, it is apparent that as strength is pushed upward, toughness of a particular high-strength alloy usually drops off quite rapidly.

It is well documented that in most instances high-strength alloys do not exhibit distinct ductile-to-brittle transitions and generally fail by plastic fracture, often referred to as dimpled rupture, fibrous fracture, or ductile fracture. Under loading conditions which impose high degrees of constraint on the high-strength alloy, such as in thick sections or at the tips of crack-like flaws, fracture may occur in a brittle manner at drastically reduced levels of nominal stress and macroscopic plastic strain with very little energy absorption.[1] The amount of energy absorbed decreases significantly as the material is strengthened to progressively higher levels.

While limited research has been done to understand the dimpled rupture process,[2,3] these studies did not deal with changes in toughness caused by varying yield strength without varying inclusion distribution. The study of a single material strengthened to several levels should provide the means by which to understand the role of microstructure on the inverse relationship between strength and toughness. The aging response of 18 Ni maraging steels has been analyzed without observations on how the microstructure and the strength affect the fracture mechanism. In this investigation the strength of an 18 weight percent Ni, 300 grade maraging steel has been systematically varied, the microstructural changes identified, and the effects of these changes on the fracture toughness and mode of fracture of this alloy have been examined. Since fracture occurs by the dimpled rupture process, the relative amounts and timing of the three generally recognized stages of the process, namely: void initiation, void growth, and void coalescence, have been studied in detail. The 18 Ni, 300 grade maraging steel has been chosen since it can be aged to an extensive range of strengths with an accompanying range in toughness. An investigation of this commercially significant material may also help in the understanding of the strength-toughness behavior of other high-strength alloys. With an understanding of the interrelationship of strength and toughness, suggestions might be made on how to modify the composition and microstructure of the 300 grade maraging steel so as to improve the fracture toughness without a significant trade-off in strength.

SCOPE OF THIS INVESTIGATION

It is the purpose of this investigation to systematically vary the strength of an 18 weight percent Ni, 300 grade maraging steel, isolate any attending microstructural changes and study the effects of these changes on the fracture toughness and mode of fracture of this alloy. The most reasonable approach to obtain material with a wide range of toughness would be to study a single heat of commercial 18 Ni, 300 grade maraging steel aged to several strength levels including underaged, fully aged, and overaged conditions. It should be noted that the as-received material contains second-phase impurity inclusions of several types. Each type of inclusion that exists in the material is present in a range of sizes which can be characterized as a size distribution with appropriate average particle diameter and variation about the average. These same populations of inclusions are present in material at all strength conditions considered in this study since aging treatments cannot alter the inclusions. The only variables are the strengthening precipitates, the yield strength, and the resulting material flow properties which will affect the resistance of the material to failure in the presence of inclusions and precipitates. Yield strengths considered range from 718 MN/m^2 (104 ksi) for the solution annealed condition to 2070 MN/m^2 (300 ksi) for the fully aged condition. The microstructure of the material at each strength level was characterized by optical metallography and thin-

foil transmission electron microscopy (TEM). Tensile properties were determined for all strength conditions. The plane strain fracture toughness (K_{Ic}) of each material was measured at room temperature with the exception of the solution annealed material which was much too tough for K_{Ic} determination in 5.1-cm (2.0-inch) thick plate.

The fracture mechanism of these microstructures was investigated through the use of fractography and sectioning techniques.[4] In order to study the progression of the fracture process at each strength level considered, several smooth, round tensile bars of each material were uniaxially deformed to increasing levels of strain up to and including that required for fracture. At each level of strain, the tensile specimens were sectioned longitudinally and examined to determine the extent of void nucleation, sizes of voids present to measure growth, and the degree and mechanism of void coalescence. With the combined use of sectioning techniques and fractography, direct identification of microstructural features which participate in the fracture process can be made and the details of the fracture appearance rationalized by an understanding of the events leading to final rupture. With these techniques, the effects of strength and microstructural changes on the relative timing and amounts of void initiation, void growth, and void coalescence can be made.

MATERIAL AND MICROSTRUCTURES

Two inch thick 18 Ni, 300 grade maraging steel of commercial purity was made in a regular mill production heat.

5

The material was produced using vacuum induction melting, cast into a round electrode, and then vacuum arc remelted. Subsequent hot working of the ingot was accomplished in two steps, the first of which involved press forging. After surface conditioning the plate material was reheated and hammer forged to the final 2-inch thickness. The material was annealed at 815°C (1500°F) and air cooled, leaving the maraging steel in the soft or unaged condition. Material variously aged to several strength levels came from this single plate of maraging steel.

The chemical specifications for 18 Ni, 300 grade maraging steel, the heat, and check analyses for the program alloy are given in Table I. The compositions are within the specifications. The check and heat analyses of the program alloy are in reasonable agreement based upon the expected error in the heat analysis. It is important to note the major elements that are intentional additions and those that are present as impurities. Specifically, Ni, Mo, Co, and Ti alloy additions are all approximately in the middle of their desired ranges. The principal impurity elements, C, S, and P are well below the maximum allowable contents. Particularly, the C and S contents are at one-tenth and one-half their maximum allowable levels, respectively.

Since it was desired to investigate the fracture behavior of the 18 Ni, 300 grade maraging steel as a function of yield strength, the age-hardening characteristics of this material were determined. By variation of both aging time and temperature, mechanical test specimens could then be aged

TABLE I

Chemical Analysis of 300 Grade,
18 Ni-Co-Mo-Ti Maraging Steels
(Weight Percent)

	Commercial Specification	Program Heat Mill Analysis	Program Check Analysis*
C	0.03 Max	0.003	0.002 ± 0.002
Mn	0.10 Max	0.02	0.04 ± 0.01
Si	0.10 Max	0.01	0.03 ± 0.01
S	0.010 Max	0.006	0.005 ± 0.001
P	0.010 Max	0.001	0.005 ± 0.001
Ni	18.0/19.0	18.29	18.53 ± 0.01
Mo	4.6/5.2	4.93	4.77 ± 0.05
Co	8.5/9.5	8.98	8.63 ± 0.1
Al	0.05/0.15	0.10	0.12 ± 0.002
Ti	0.5/0.8	0.63	0.65 ± 0.01
Zr	0.02 Added	0.016	0.015 ± 0.001
B	0.003 Added	<0.001	<0.001 ± 0.001
Ca	0.05 Added	-	0.025 ± 0.01
N_2	-	-	0.005 ± 0.001
Fe	Balance	Balance	Balance

*Average from two separate test blocks

to attain specified strength levels. An isothermal aging study was carried out. Figure 1 is a plot of Rockwell "C" hardness as a function of the logarithm of time at each of the aging temperatures shown. The annealed or solution treated material represents the lowest hardness at zero time of about Rockwell "C" 30. As with most age-hardenable alloys, the 300 grade maraging steel rapidly overages at a high temperature such as 538°C (1000°F). Although kinetically less rapid, aging at lower temperatures yields a maximum hardness which is greater than that attained at higher temperatures. In this system, loss of hardness (strength) due to overaging is due in part to classical precipitate coarsening and to a time-dependent reversion of the metastable body-centered cubic martensite to the equilibrium face-centered cubic austenite.[5] Ultimately, specimens aged for 50 hours at 371°C (700°F), 3 hours each at 427°C (800°F), 482°C (900°F), and 538°C (1000°F), and for 100 hours at 427°C (800°F) were tested for valid plane-strain K_{Ic}. Tensile strength and ductility of the solution treated material was studied along with the above conditions even though K_{Ic} could not be measured for this low strength material.

The variation in microstructure as a function of aging treatment was examined using optical metallography, surface replica TEM, thin-foil TEM, and X-ray diffraction techniques. Specimens for optical metallography were mechanically polished and etched in a Kalling's reagent, $CuCl_2$ and HCl in methanol and H_2O. The etching procedure provided excellent contrast to reveal the lath martensitic structure. With etching there

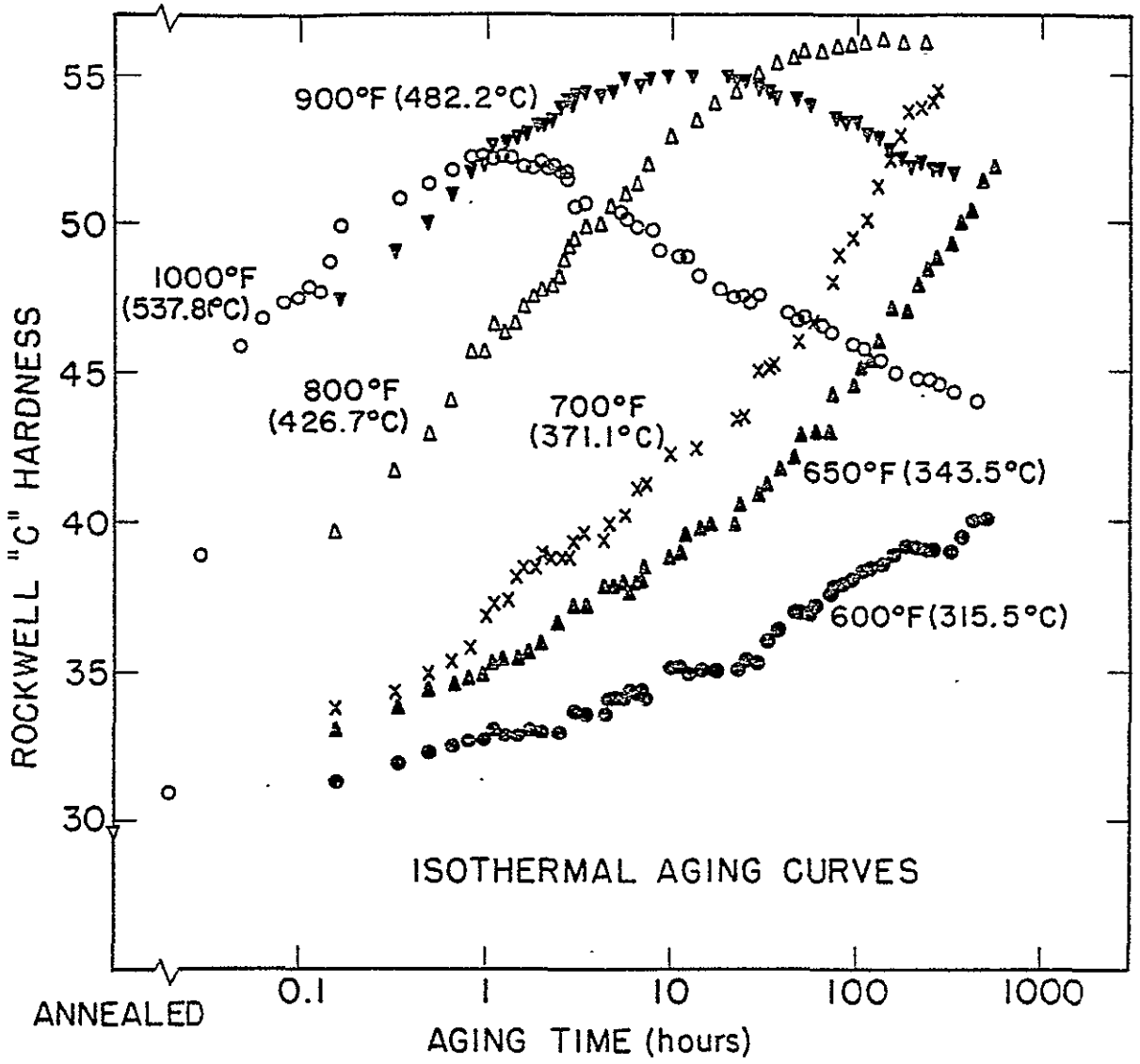

Figure 1 Hardness versus logarithm of time at temperature for some of the aging treatments used on the 18 Ni, 300 grade maraging steel.

was a tendency to obscure the inclusions, however, this was unimportant since adequate contrast existed in the unetched condition for the optical metallography of inclusions. Thin foils for TEM were electropolished by a standard window technique using an electrolyte of sodium chromate in glacial acetic acid.

Figure 2 shows an optical micrograph of the polished and etched structure aged at 482°C (900°F) for 3 hours. The annealed and underaged strucutres do not show any significant difference in lath morphology as revealed by optical metallography and for that reason are not shown in Figure 2. The grain structure of the maraging steel has a well-developed Widmanstätten-like morphology. The intercept grain size as revealed in Figure 2 is 22.7 ± 3.1 μm (about ASTM grain size No. 8).

Unlike the annealed or conditions up to and including the fully aged material, with overaging there is a tendency to form the equilibrium austenite phase within the aged body-centered cubic lath martensite structure. Overaging in the material aged for 3 hours at 538°C (1000°F) is apparently due to a combination of classical precipitate coarsening and softening due to the formation of austenite.[6] Although the presence of cobalt in the maraging alloy tends to suppress the formation of equilibrium austenite to higher temperatures to allow sufficient precipitation of Ni-Mo rich particles, significant amounts of austenite will form in short times at aging temperatures above 482°C (900°F). As shown in Figure 3, austenite tends to form at both prior austenite grain

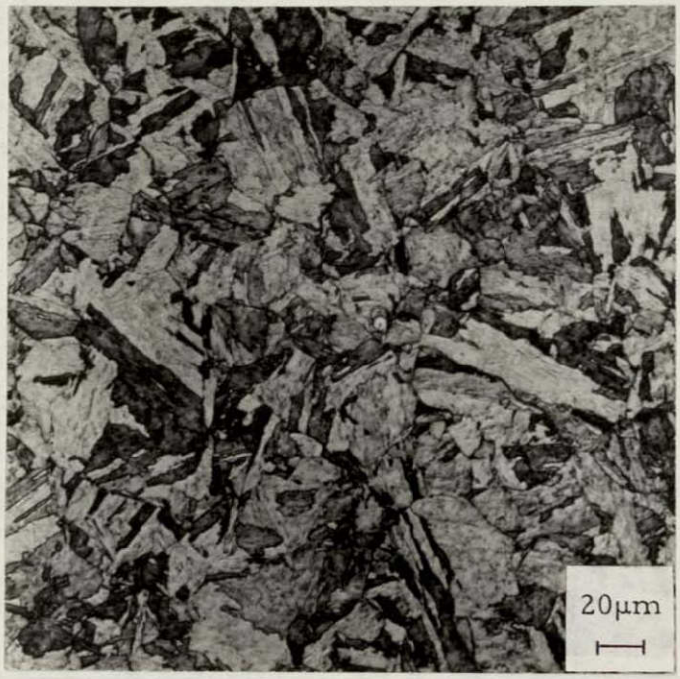

Figure 2 Optical micrograph of polished and etched section of 18 Ni, 300 grade maraging steel

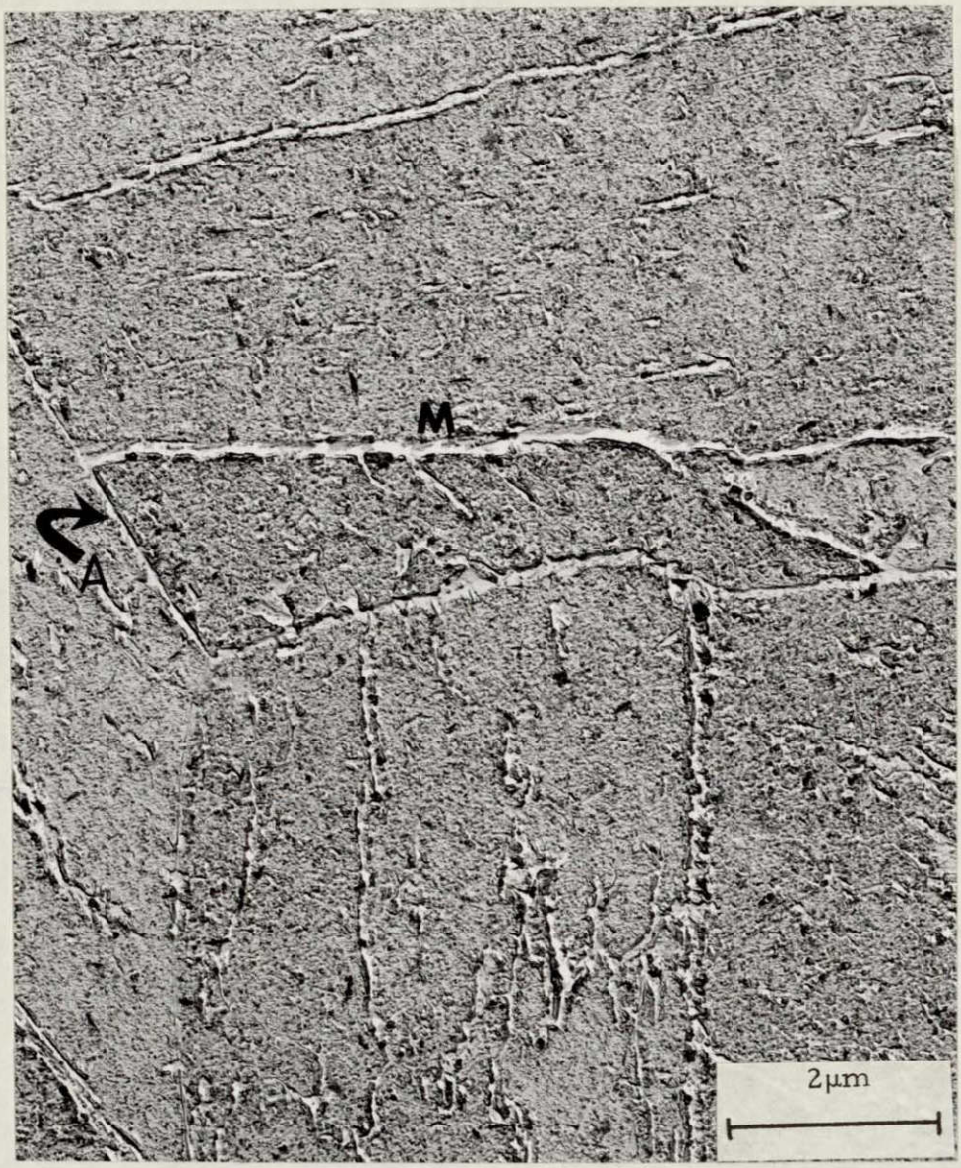

Figure 3 TEM replica micrograph of reverted austenite outlining prior austenite grain boundaries (marked A) and martensite lath boundaries (marked M).

boundaries and lath martensite boundaries. Approximately 4.2% austenite by volume was present in the overaged material.

The changes in the fine internal structure of the 18 Ni, 300 grade maraging steel which occur with different aging conditions were studied by thin-foil TEM. The underaged, fully aged, and overaged microstructures included the annealed or solution treated condition as a base material. Underaged materials include the 50-hour, 371°C (700°F) and the 3-hour, 427°C (800°F) treatments. The commercial aging treatment of 3 hours at 482°C (900°F) was considered which is also underaged relative to the material given a 100-hour treatment at 427°C (800°F). The overaged structure considered was produced by aging for 3 hours at 538°C (1000°F). The thin-foil specimens were examined at 100 kv. The precipitate phases were identified with the aid of a computer program[7] that resulted in the calculation and listing of d-spacings and angles between planes for the tetragonal, orthorhombic, and hexagonal systems when the computer was supplied with the appropriate lattice parameters.

Figure 4 shows a thin-foil TEM brightfield micrograph for the solution treated material. Shown in this micrograph is a lath structure with a very high density of dislocations. The structure, which as expected is precipitate-free lath martensite, can be indexed as a bcc material. Some dislocation rearrangement associated with a deterioration of the martensite lath subboundaries occurs upon aging at 371°C (700°F) for 50 hours or at 427°C (800°F) for 3 hours. Although the strengths of these two materials are twice that

in the solution treated condition, there were still no resolvable precipitates in the brightfield images. The bcc SAD patterns from material aged at 427°C (800°F) for 3 hours frequently show some streaking which may result from extremely fine and non-resolvable coherent precipitates. This is believed possible when the work of Rack and Kalish[8] is considered wherein an aging treatment at 427°C (800°F) for 3 hours in a 350 grade maraging steel produced an extremely fine precipitate. It is possible that the initial stages of precipitation in the 300 grade steel are evidenced by streaking and not by distinct spots because of low volume fraction, particle coherency, and particle sizes approaching the resolution limit of the electron microscope.

Precipitation is apparently similar in the materials given the commercial aging treatment at 482°C (900°F) for 3 hours and the maximum hardening treatment at 427°C (800°F) for 100 hours. The brightfield TEM micrograph in Figure 5a of material aged for 100 hours at 427°C (800°F) shows clearly resolved precipitates that are about 500 Å at maximum length. The dark field image in Figure 5b is taken from the spot marked $(12\bar{1})_p$ in the schematic of Figure 6b. The bcc lath martensite SAD pattern is from a $[31\bar{1}]$ matrix zone axis. The precipitates which have come about due to the $(12\bar{1})_p$ spot are rod-shaped orthorhombic Ni_3Mo with a zone axis of $[5\bar{3}1]$. Because there are extra spots in the SAD pattern shown in Figure 6a, the presence of a tetragonal sigma phase is suggested but this was never confirmed since these spots were too weak

Bright field image

Figure 4 Thin foil TEM of Lath structure in solution treated material.

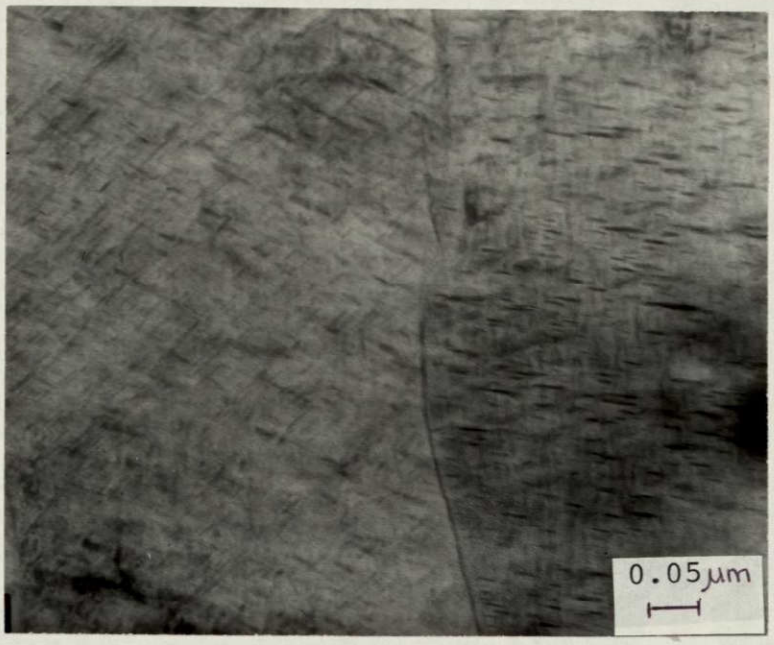

(a) Bright field image

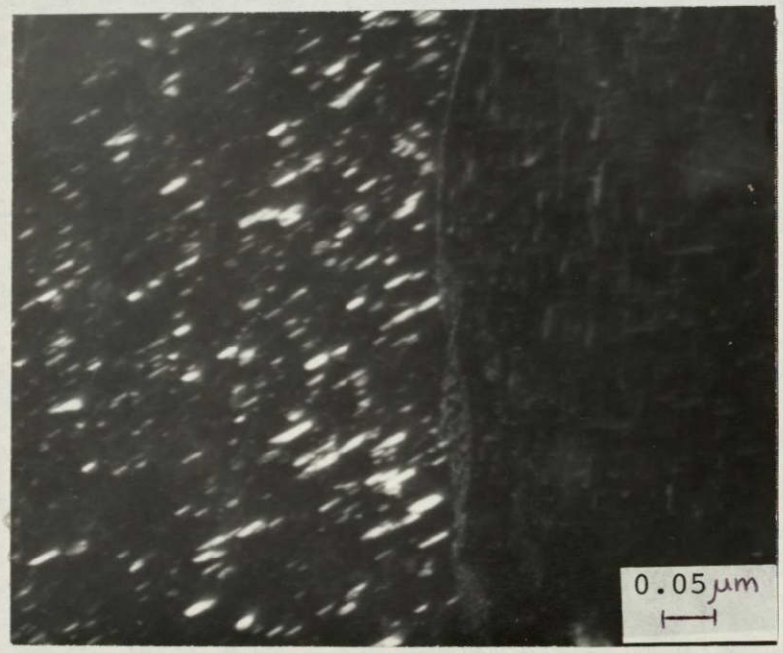

(b) Dark field image from the (121)p reflection in Figure 6 (b).

Figure 5 TEM micrographs showing the structure of the Ni_3Mo precipitates in material aged for 100 hours at 800°F (427°C).

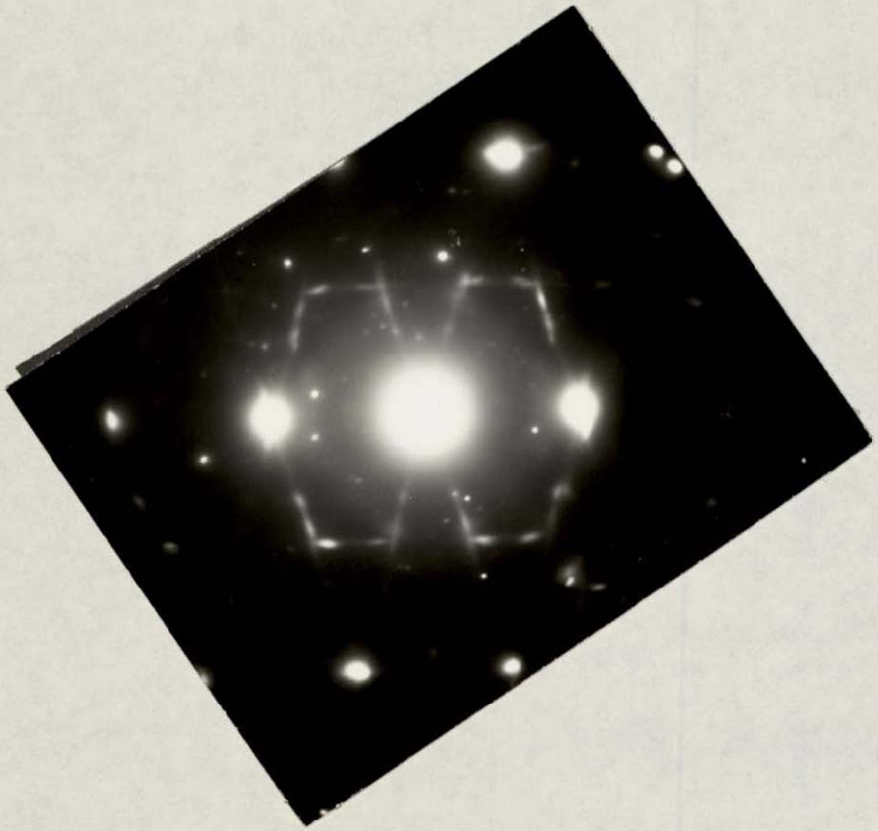

(a) SAD pattern

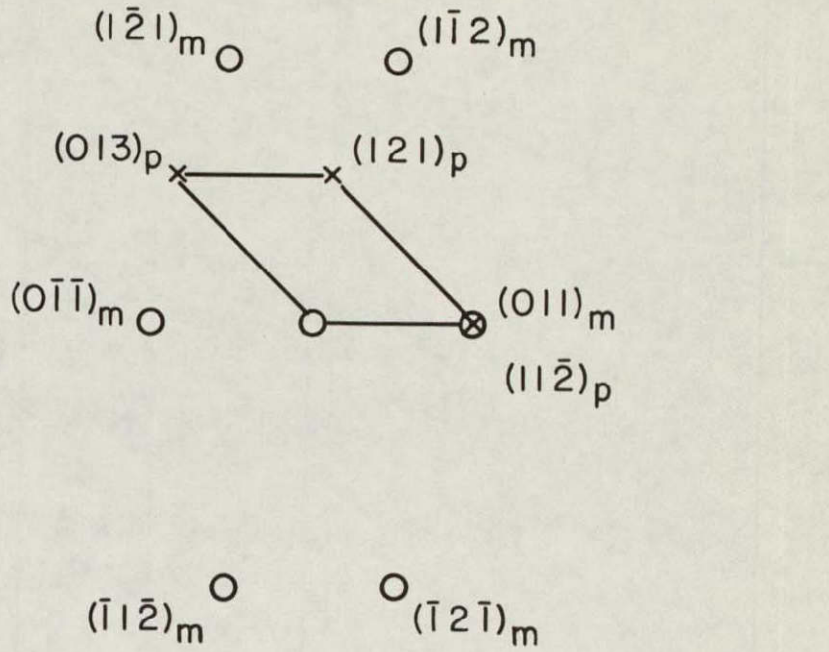

(b) Schematic

Figure 6 Diffraction pattern and schematic from bcc Lath martensite $[3\bar{1}\bar{1}]$ Zone and Ni_3Mo precipitates from an Orthorhombic $[5\bar{3}1]$ Zone Axis.

in this case to give dark field images. The works of Spitzig, Chilton, and Barton[9] in 300 grade maraging steel and Rack and Kalish[8] in 350 grade maraging steel show supportive evidence to this contention. These authors,[8,9] also lack conclusive evidence due to the complexity of the 18 Ni maraging steel systems as well as the similarity in the Ni_3Ti, Fe_2Ti, FeTi or even NiTi structures.

The existence of strengthening precipitates in the commercially and fully aged structures cannot be disputed. After aging at 482°C (900°F) for 3 hours, the precipitates are about 200-300 Å long on the average. After aging for 100 hours at 427°C (800°F), precipitation appears to be more dense and the average precipitate length approaches 400-500 Å. Overaging at 538°C (1000°F) for only 3 hours primarily results in Ni_3Mo precipitate coarsening. Most of the rod-shaped Ni_3Mo precipitates present in the fully aged condition are now much larger ellipsoids. Occasionally, small spheres of Fe_2Mo have been shown to exist in the overaged microstructure.[8] It will be shown later in the fractography and sectioned tensile specimen sections that the precipitates in the fully aged and overaged materials act as sites for void formation during the void coalescence process of fracture.

NON-METALLIC INCLUSIONS

It is well documented that in many high-strength alloys, second-phase impurity inclusions are the sites for void nucleation.[3] In order to define the exact nature of the inclu-

sions in 300 grade maraging steel, a metallographic investigation was carried out. Polished, unetched metallographic sections were examined from each of three orthogonal directions, the axes being defined using ASTM E399-74 terminology[10] as the length, L (the major forging direction in this case); long transverse, T (the plate width); and the short transverse, S (the through thickness). There are three types of second-phase impurity inclusions present in the 300 grade maraging alloy. Based upon their appearance in the optical microscope and comparison with descriptions from previous inclusion studies, the large inclusions were tentatively identified as titanium carbonitrides (Ti(C, N)) and titanium sulfides (Ti_2S).[11] The third type of inclusion identified as TiC, is about one-tenth the size of the larger particles.[12] The most prevalent shapes of the large inclusions are shown in Figure 7. The fine TiC inclusions are not shown in Figure 7. The TiC inclusions are best revealed optically by mechanically overpolishing the material but not etching since the lath structure will then obscure the inclusions.[12] Mechanical overpolishing was usually avoided, however, so as to preserve the large inclusions and prevent pitting. The smaller TiC inclusions will be shown below.

The micrograph in Figure 7 was taken from the LT plane. The inclusions that appeared as sections from cubes and sometimes rounded are pink in color and are believed to be Ti (C,N). As shown in Figure 7, the elongated and the cuboidal inclusions are often in contact with one another. The cubes

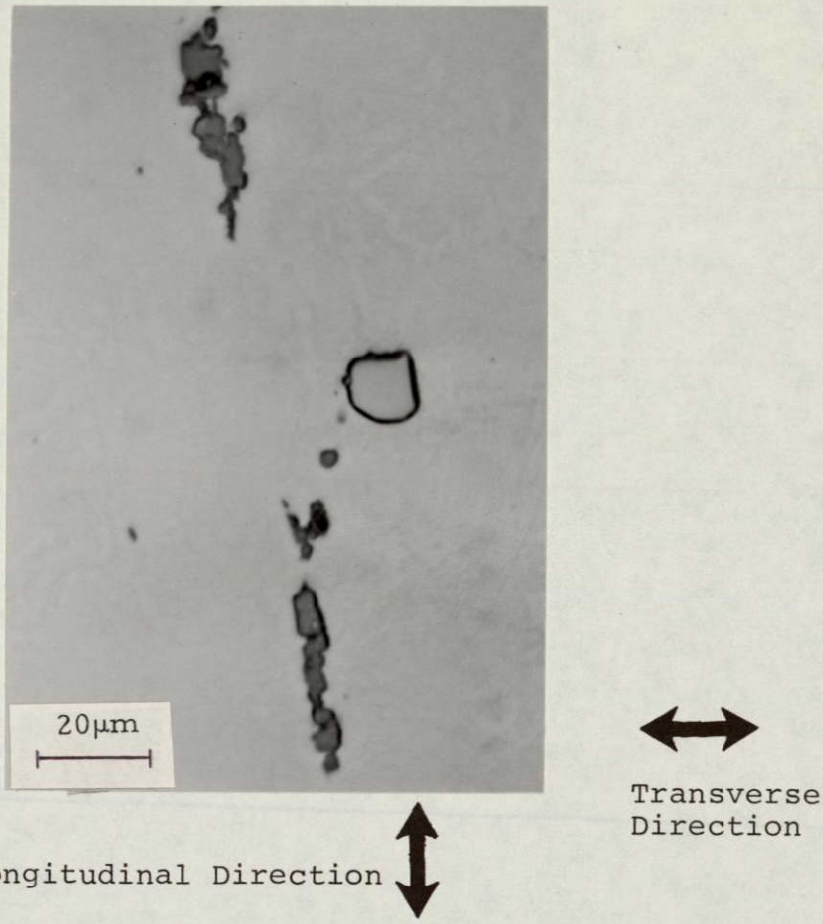

Figure 7 Optical micrograph of the most prevalent large inclusions in the 18 Ni, 300 grade maraging steel.

did not appear to have been plastically deformed during the hot-forging operations but were sometimes cracked from forging. The elongated and irregular inclusions appearing dark gray in Figure 7 are similar to the Ti_2S particles observed in a previous investigation.[11] Since the irregular inclusions are elongated in the forging direction, they were undoubtedly plastically deformed and sometimes cracked during the hot-forging operations. An equivalent number of precracked inclusions were still evident in electropolished sections which proved that the mechanical polishing operation did not damage the inclusions. Comparison of these optical metallographic observations with those of previous investigations[11,12] together with X-ray data from the SEM showing that the cubes were rich in titanium identified these inclusions as titanium carbonitrides, Ti(C, N). Since the elongated inclusions were rich in titanium and sulfur they were identified as titanium sulfides, Ti_2S. The cuboidal inclusions are usually much less than 10 μm on edge. The elongated inclusions are frequently 20 μm long and usually less than 10 μm in width.

After careful mechanical overpolishing, it becomes obvious that a third, fine inclusion population is present uniformly distributed throughout this heat of 18 Ni, 300 grade maraging steel. The material is relatively dilute with respect to the Ti(C, N) and Ti_2S inclusions but the fine background inclusions are present in a much higher volume fraction. The relative size and population of the fine inclusions is shown in Figure 8. Since these inclusions were,

on the average, less than 1 μm in diameter, extraction replica TEM and selected area electron diffraction techniques were used to identify these particles. Based upon similar particles having an fcc crystal structure,[12] these inclusions were thought most probably to be TiC. The calculated lattice spacings of the planes within the extracted particles producing the fcc patterns were compared with the reported d spacings of TiC from the work of Nes and Thomas.[12] From the excellent correlation, it was concluded that these fine inclusions were titanium carbides, TiC.

A quantitative metallographic investigation was undertaken to assess by type the number, spacing, and size distribution of the second-phase impurity inclusions in this material. From the extracted TiC particles, it was concluded that for all practical purposes these inclusions were cuboidal. The Ti_2S and Ti(C, N) were treated as ellipsoids and cubes, respectively. The quantitative metallographic treatment of the Ti(C, N) and TiC shapes are due to Hull and Houk[13] and Meyers[14] and to DeHoff and Rhines[15,16] for the ellipsoidal Ti_2S shape. For each type of particle, the total number of inclusions and the fraction of those which were cracked or separated at the particle-matrix interface were counted per unit area. The average inclusion size was determined along with a size distribution from the measurement of more than a thousand inclusions of each type of particle.

The single heat of commercial 300 grade maraging steel which contains three types of second-phase inclusions has been characterized and results are summarized in Table II.

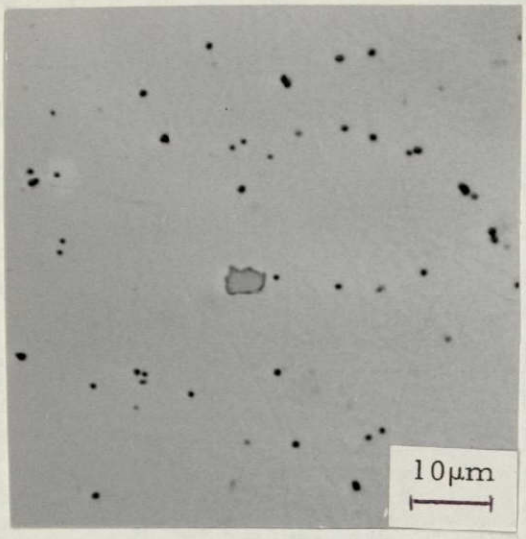

(a) Optical micrograph of TiC inclusions

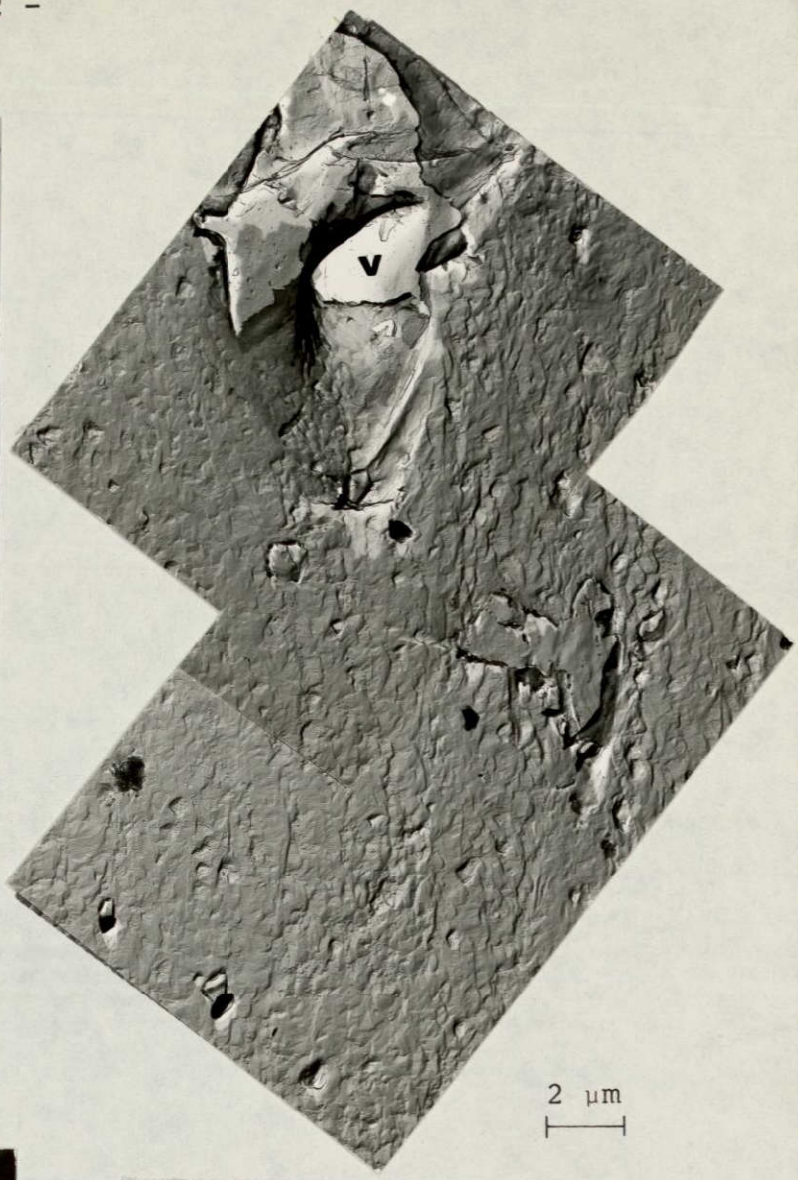

(b) TEM replica micrograph of deformed and etched tensile specimen (Tensile axis vertical)

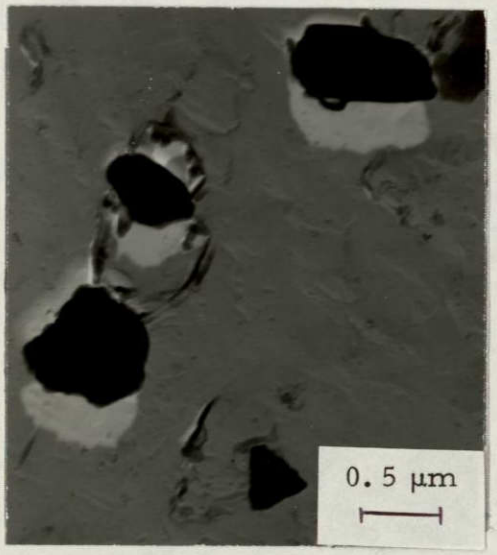

(c) Extracted TiC inclusions

(d) [111] Zone Axis of fcc TiC structure

Figure 8 Micrographs of the fine background inclusions and identification as TiC. (replicated void marked "v")

The limits given for each reported value represent plus and minus one standard deviation about the average. Included in the table are, by type, measurements of particle size, number per unit volume (N_V), volume fraction (V_V), and center-to-center spacing between particles in a volume of material (3D) and on a planar view (2D). The maraging steel matrix is most clean with respect to Ti(C, N) and then Ti_2S inclusions. Note that the N_V of Ti(C, N) inclusions is roughly two orders of magnitude lower than N_V for the Ti_2S inclusions. In turn, the density of fine TiC inclusions is about four and two orders of magnitude larger than the N_V for the Ti(C, N) and Ti_2S inclusions, respectively.

The size of the average TiC inclusion is about ten times smaller than either the Ti(C, N) or Ti_2S. The apparent trade-off between size and number per volume is evidenced by the relative volume fractions. The volume fraction of TiC inclusions is nearly four times greater than that for the Ti_2S inclusions and about fifteen times greater than the Ti(C, N) particle fraction. The center-to-center spacing ($\bar{\lambda}$) of inclusions follows some inverse relation of the number per unit volume, namely, the interparticle spacings are greater for the most dilute species, Ti(C, N). The next largest spacing is between nearest neighbor Ti_2S with the TiC particles spaced only a few microns apart. As may be seen from the $\bar{\lambda}$ data, the variability of the various measurements is quite high. Along with the experimental difficulties in measuring particles in an opaque volume of material, the large scatter in the Ti(C, N) and Ti_2S spacing data is due to the tendency

TABLE II

Results of Quantitative Metallographic Investigation of the Three Types of Inclusions in 18 Ni, 300 Grade Maraging Steel

Inclusion Type	Inclusion Size (μm) $\bar{d}_L$ or $\bar{a}$	$\bar{d}_T$	$\bar{d}_S$	Center-to-Center Spacing (μm) 2D	3D	N_v Inclusions / cm^3	V_v Volume Fraction (%)	Inclusions Voided at Strain "0" (%)
Ti(C, N)	3.3 ± 1.7	-	-	112.1 ± 28.5	20.2 ± 8.1	$3.1 \times 10^5 \pm 1.9 \times 10^5$	0.08 ± 0.02	5.0
Ti_2S	5.6 ± 3.6	3.5 ± 2.4	2.2 ± 1.0	55.2 ± 11.1	15.3 ± 8.8	$2.9 \times 10^7 \pm 1.2 \times 10^7$	0.24 ± 0.13	19.0
TiC	0.39 ± 0.2	-	-	5.4 ± 0.9	3.2 ± 0.4	$5.8 \times 10^9 \pm 2.3 \times 10^9$	0.99 ± 0.36	0

for these particles to cluster in stringers. The percent scatter about the average TiC spacing data is much less since these inclusions are much more homogeneously distributed in the material. For these reasons, the Ti(C, N) and Ti_2S average inclusion spacing values are less meaningful. The volumetric ($\bar{\lambda}_{3D}$) center-to-center spacing between nearest neighbor inclusions (all three types of particles included) is only 3 μm which correlates well with the closely spaced voids and, in turn, fine dimples on the fracture shown below. Note also that with a combined volume fraction (V_V) of 1.3% inclusions in this heat of 300 grade maraging steel, the material is much less clean than the commercial 200 grade maraging alloy studied by Cox and Low.[3] Their material contained only Ti(C, N) inclusions at a volume fraction of 0.21%. Combined, the Ti(C, N) + Ti_2S total volume fraction yields 0.32% inclusions in the 300 grade material. The most striking difference is the presence of fine TiC inclusions which account for the additional 1 volume % impurity particles. Included in Table II are % voided values for each particle type in the as-received plate which serve to rate the integrity of the inclusion before deformation. Although none of the fine TiC inclusions have detectable voids, a significant number of Ti(C, N) and Ti_2S inclusions have cracks in them with 5% and 19% voided at zero strain, respectively.

It is generally expected that the largest inclusions in the material will form the first voids as deformation proceeds. To realistically expect to test this hypothesis as a

function of material strength, more information about the inclusions is needed than the average diameter and deviations from the mean. The scatter about the average diameters clearly indicates that there are distributions of particle sizes for each of the three types of inclusions. Since it is also expected that smaller and smaller particles will form voids as the amount of deformation is increased, the average value will not be sufficient to describe the fracture process. The relative size shift between the Ti(C, N), Ti_2S, and TiC inclusions can be followed in Figure 9 by comparison of distribution curves one above the other since the diameter scales are equivalent. The most important fact to remember from Figure 9 is that this set of size distribution curves characterize the three populations of inclusions which exist in a single heat of 300 grade maraging steel. Further, these same distributions are characteristic of the inclusions in the material at all strengths considered in this study. The exact portion of these size distributions that contribute to void formation and fracture is dependent upon the matrix strength level.

MECHANICAL PROPERTIES

The room temperature mechanical properties of the commercial heat of 300 grade maraging steel were characterized using smooth, round bar tensile tests, fatigue precracked Charpy impact tests, and plane-strain fracture toughness, K_{Ic} tests. These properties were examined as a function of strength level in the single heat of maraging steel in the

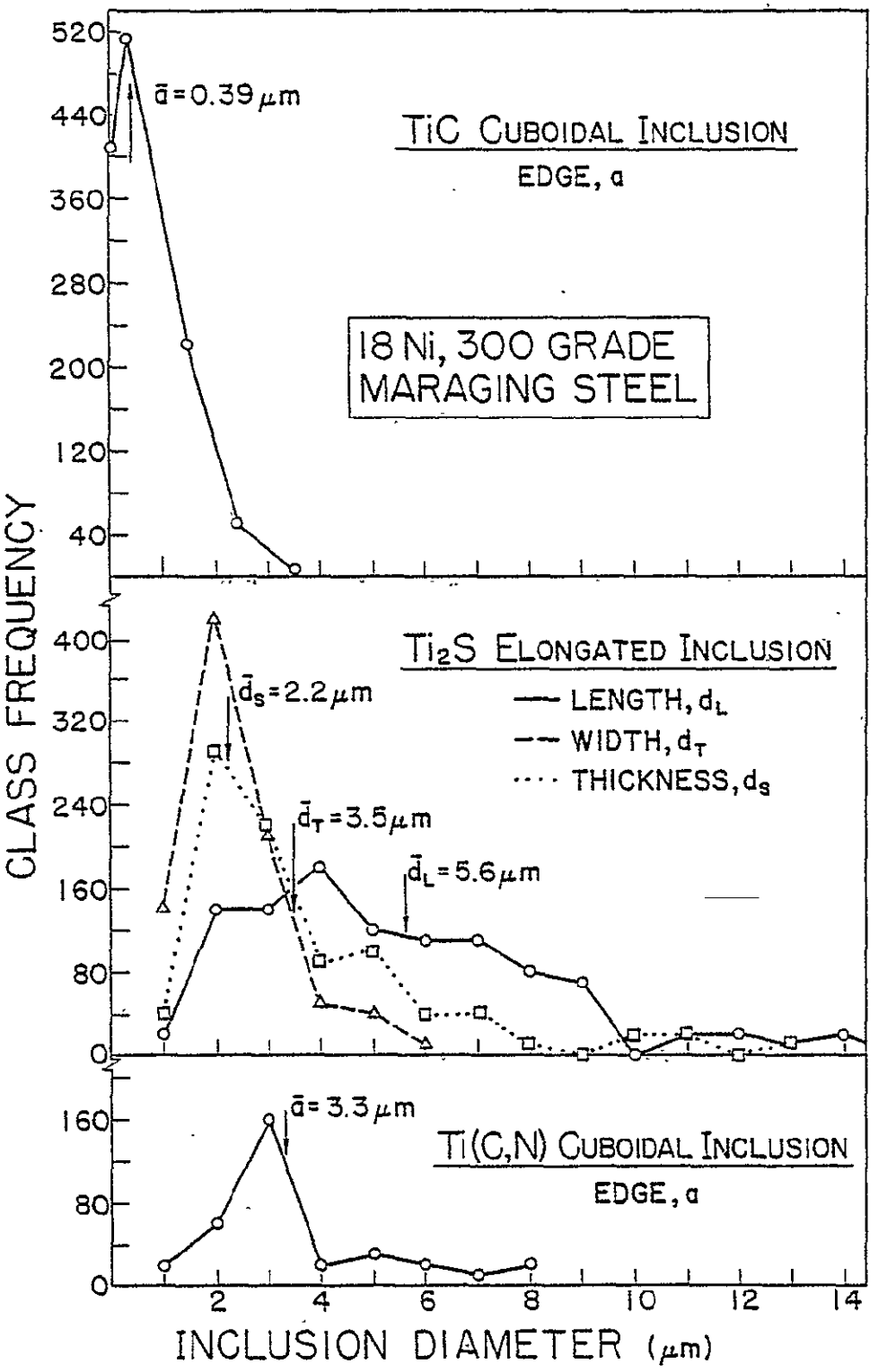

Figure 9 Size distributions for the Ti(C,N), Ti_2S, and TiC inclusions in the 18 Ni, 300 grade maraging steel.

solution treated condition as well as in the aged conditions listed in Table III. The fatigue precracked Charpy impact tests were performed as an initial measure of the magnitude of the strength-toughness trend to permit a more judicious choice of conditions for valid K_{Ic}. The estimated K_Q values in Table III were calculated from the total energy lost in impact per unit uncracked area, W/A, involved in fracture.[17] The K_{Ic} testing was carried out using both compact tension specimens and bend specimens in accordance with ASTM Standard E399-74.[18] The fracture toughness and Charpy impact specimens were tested in the LT orientation. In LT orientation fracture toughness specimens, the crack plane is perpendicular to the plate longitudinal direction and the crack propagates in the transverse direction so the plane of fracture had the same orientation in all specimen geometries. The details of the techniques and test results have been described elsewhere.[19] The toughness value for the material aged at 371°C (700°F) for 24 hours is invalid due to the susceptibility of the material to intergranular subcritical crack growth in this condition. Although the details[19] of subcritical crack growth in the 300 marage material are of practical importance, this microstructure was avoided so as not to further complicate the strength-toughness trend.

It can be seen from Table III that the aging treatments used have established an extensive range of strength levels. Based upon a comparison of yield strengths, the 100-hour, 427°C (800°F) material is about 1350 MN/m^2 (196 ksi) stronger

TABLE III

Mechanical Properties of 18 Ni, 300 Grade Maraging Steel

Room Temperature Tests
(Data indicates the mean ± one standard deviation)

Aging Temperature °F (°C)	Aging Time (hrs.)	σ_y 0.2% Yield Strength (ksi) (a)	Ultimate Tensile Strength (ksi) (a)	Fracture Strain	Precracked Charpy Estimated K_Q (ksi/in.) (b)	K_{Ic} (ksi/in.) (b)
Solution Treated	-	104.1 ± 0.0	145.2 ± 0.2	1.558 ± 0.007	351.5 ± 5.2	-
700 (371)	24	195.1 ± 0.9	215.2 ± 0.6	0.951 ± 0.007	116.7 ± 2.3	167.1 (c)
700 (371)	50	209.0 ± 0.2	228.7 ± 0.2	0.836 ± 0.057	89.2 ± 5.5	129.8 ± 2.9
800 (427)	3	225.1 ± 0.4	239.1 ± 1.9	0.778 ± 0.022	94.2 ± 3.0	96.6 ± 7.0
900 (482)	3	268.8 ± 1.3	278.9 ± 1.0	0.742 ± 0.010	91.2 ± 3.8	78.2 ± 0.4
1000 (538)	3	246.3 ± 0.4	259.8 ± 1.6	0.635 ± 0.020	90.4 ± 2.7	66.7 ± 1.8
800 (427)	100	299.6 ± 1.5	308.4 ± 0.7	0.468 ± 0.021	60.1 ± 0.6	50.9 ± 0.2

(a) 1 ksi = 6.9 MN/m^2

(b) 1 ksi/in. = 1.1 $MN/m^{3/2}$

(c) This result is invalid due to subcritical crack growth behavior of material in this condition.

than the solution treated material. A strength range comparison for which valid K_{Ic} measurements have been made might be more realistic to consider. Assuming the 371°C (700°F), 50-hour aging treatment results in the lowest strength for valid K_{Ic}, a variation in strength of about 628 MN/m^2 (91 ksi) is available for investigation. With increasing strength and/or overaging, the valid K_{Ic} data show a decrease of nearly 88 MN/m$^{3/2}$ (80 ksi $\sqrt{\text{in.}}$).

A plot of strength versus toughness is given in Figure 10. In this figure are plotted valid K_{Ic} against the 0.2% offset yield strength data. These data are averages of at least three tests per condition. The error bars indicate the range of plus and minus one standard deviation (68 percent confidence limits). Where error bars are not shown, the standard deviation is smaller than the point representing the average value. The fine lines in Figure 10 that are marked B = 0.394, 0.75, etc. establish the maximum K_{Ic} that can be measured in a valid manner with that specimen thickness for a given yield strength material. These lines at various values of B are equal to the ASTM requirement[10] of 2.5 $(K_Q/\sigma_Y)^2$. Figure 10 indicates that toughness decreases with increasing strength as well as with overaging. In other words, at a yield strength of about 1725 MN/m^2 (250 ksi) the underaged material is expected to be about 22 MN/m$^{3/2}$ (20 ksi $\sqrt{\text{in.}}$) tougher than the overaged material. The continued decrease in toughness with overaging is related to the size of overaged precipitates and their role in the void coalescence process. Details of this explanation including

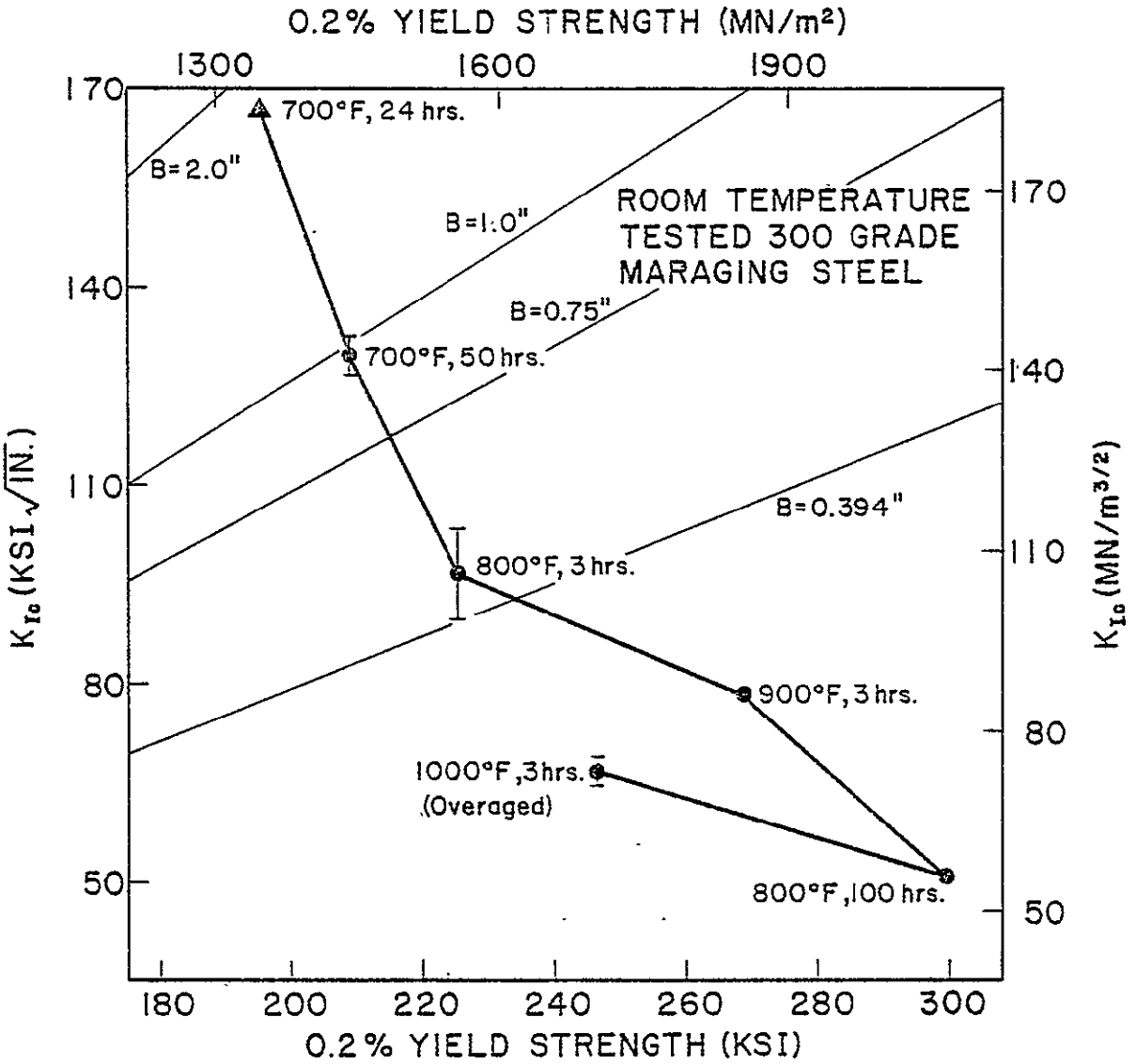

Note: ▲ K_Q value is invalid due to subcritical crack growth behavior of this microstructure and ASTM E399-74.[10]

Figure 10 Valid K_{Ic} fracture toughness of variously strengthened 18 Ni, 300 grade maraging steel tested at 20°C (68°F).

fractographic and sectioned tensile specimen evidence will be presented below. It is interesting to note that the tensile fracture strain data decrease with increasing strength and/or overaging in a similar fashion to the toughness data. For example, by increasing the yield strength from 1442 to 2067 MN/m^2 (209 to 300 ksi), K_{Ic} decreases by 60.8% and in a similar fashion, the fracture strain (ε_f) decreases by nearly 45%. This trend provides, at best, a rough indication that deformation in the tensile and K_{Ic} specimen might be comparable. In fact, the direct relationship between ε_f and K_{Ic} with strength level will be used to the advantage of the experimental tensile sectioning work reported below.

Tensile flow curves were determined for the 300 grade maraging steel for the strength levels shown in Figure 11. Note that the shape of the flow curves are surprisingly constant. By differentiating the empirical flow curves with respect to strain it was concluded that the change in work-hardening behavior with strength change over a range of 1352 MN/m^2 (196 ksi) is insignificant.

FRACTOGRAPHY

The fracture surfaces of tensile and fracture toughness specimens tested in the yield strength conditions shown in Table III were examined using two-stage TEM replicas as well as by direct observation in the SEM. At all strength levels considered, the K_{Ic} and tensile specimen fracture surfaces were rough and fibrous in appearance when viewed at low mag-

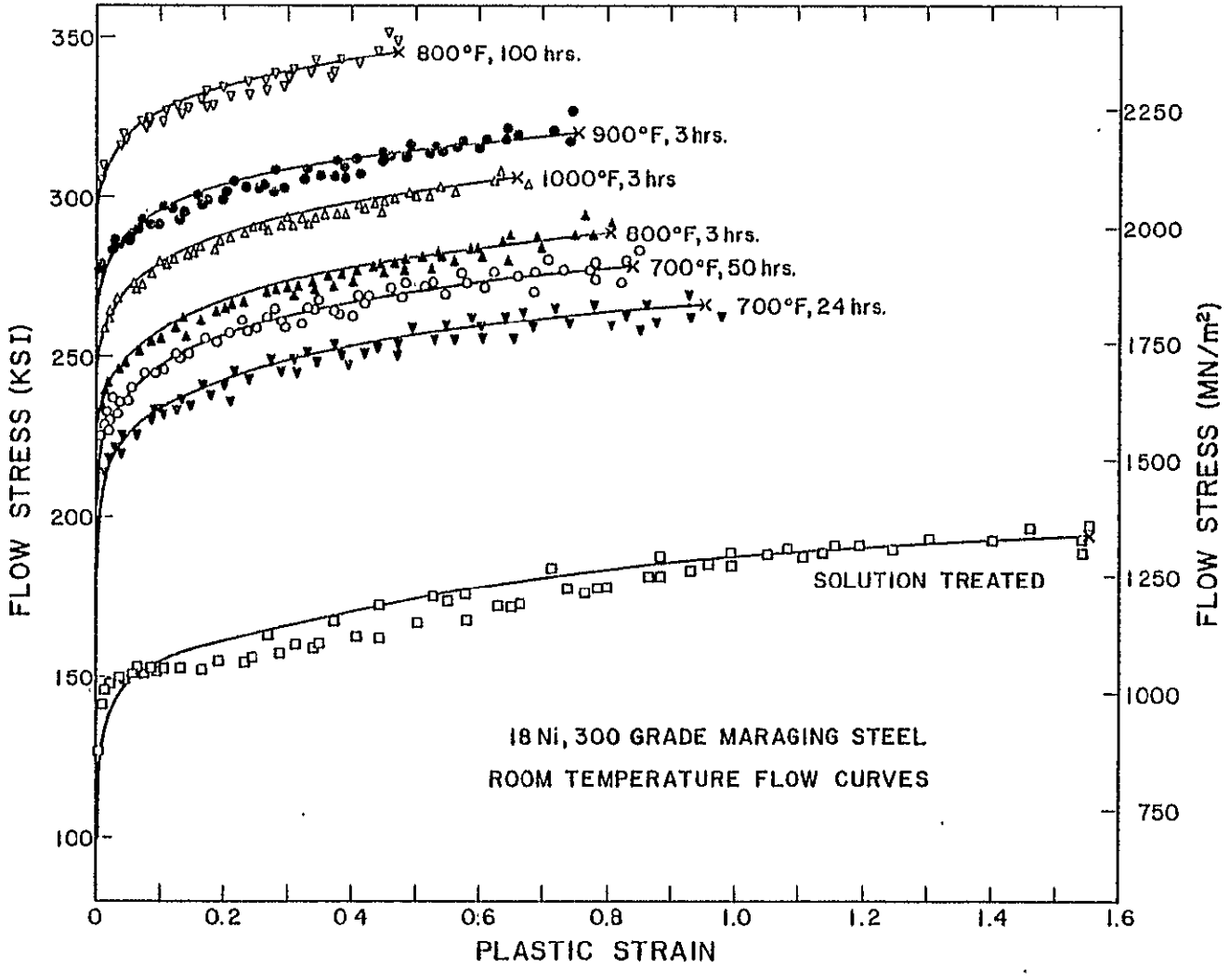

Figure 11 Room temperature tensile flow curves of variously aged 300 grade maraging steel. Solid lines are the result of the regression analysis. The "X" represents the average fracture strain.

nification. The topography of the low strength fracture was extremely rugged by comparision to the relatively flat surface of the fully strengthened tensile fracture. In general, the fracture surface roughness decreased with increasing strength.

The TEM replicas were viewed using stereo pairs and the fracture mode at all strength levels observed was dimpled rupture. Dimpled rupture is the mode of fracture whereby microscopic voids nucleate at second-phase particles, then grow and coalesce to cause final rupture. This mode of fracture is termed dimpled rupture since both halves of the fracture surface are covered by depressions, or dimples, which have formed due to void formation at a second-phase particle, void growth, and void coalescence. Based upon extensive examination of stereo pairs, it was found that by increasing the strength and/or overaging the matrix, the fracture toughness decreases accompanied by a decrease in dimple size. The number of dimples increases while the average dimple size decreases due in part to a larger fraction of the size distribution of second-phase particles that have participated in void formation. This includes dimples at the large (Ti (C, N) and Ti_2S) inclusions and also at the small TiC inclusions. With increasing strength, a larger fraction of the fracture surface appears to be covered by the voided TiC nucleated dimples. As strength is increased, the critical size impurity inclusions for void initiation decrease as evidenced by the impressions of smaller particles on fractographs of higher strength material. Tensile and

35

K_{Ic} fracture surface comparisons were made with observation of more than twenty stereo pairs for each of the 718, 1442, 1553, 1856, 1697 (overaged), and 2070 MN/m^2 (104, 209, 225, 269, 246, and 300 ksi) yield strength materials. The fracture process in this material is complex and conclusions have been drawn only after careful examination of many fractographs. The number of examples must be limited and hence only the lowest and highest yield strength material fractures will be shown here. Figure 12 shows a typical SEM fractograph from the solution treated, 718 MN/m^2 (104 ksi) yield strength tensile specimen fracture. The largest (15-20 μm) dimples have resulted from void formation at Ti(C, N) or Ti_2S inclusions. The holes around these inclusions as well as their breakup indicate that void formation occurs by a combination of inclusion-matrix interface separation and inclusion cracking. When viewed in stereo, these holes appear very deep which might account for the difficulty in stripping plastic replicas from this rough surface. Adjacent to the large inclusion nucleated dimples are 4-5 μm dimples which result from void formation at the 0.1-1.0 μm TiC inclusions.

The SEM fractograph from the fully aged, 2070 MN/m^2 (300 ksi) yield strength tensile specimen fracture is shown in Figure 13. The strengthening precipitate dimples that densely cover regions marked by the letter "P" in Figure 13 are very shallow and similar in size to those in the 1856 MN/m^2 (269 ksi) yield strength condition. These dimples are not as fine as those in the overaged material. Likewise the

strengthening precipitate dimples do not occupy as large an area of the total fracture surface since the precipitates have not coarsened to the extent that they have with overaging at 538°C (1000°F) for 3 hours. The large inclusion (Ti (C, N) and Ti_2S) nucleated dimples are smaller and occupy a much smaller area fraction of the fully strengthened fracture. This is because a larger number of TiC inclusion plus precipitate nucleated dimples cover the fully aged fracture surface than in any of the lower strength conditions. The broadest portion of the population of TiC inclusions, including many particles as small as 0.1 μm in diameter are found in the bottom of the dimples of this, the least ductile or tough material considered in this investigation. The arrrows mark the TiC inclusions which were resolved in Figure 13.

The higher resolution of TEM replica fractography (Figure 14) has clearly revealed 0.05-0.1 μm (500-1000 Å) depressions in the submicron size dimples which would indicate that precipitates are the nucleation sites for these fine dimples. Since strengthening precipitates grow with extent of aging and tend to become incoherent with the matrix, the possibility for void formation at precipitates to accelerate the coalescence of the larger voids formed earlier at Ti(C, N), Ti_2S, and TiC inclusions is entirely possible.

The fracture surfaces reviewed in Figures 12 through 14 above provide only an indirect means by which to assess the relative influence of microstructure on the fracture process. The major differences between the fracture surfaces at vari-

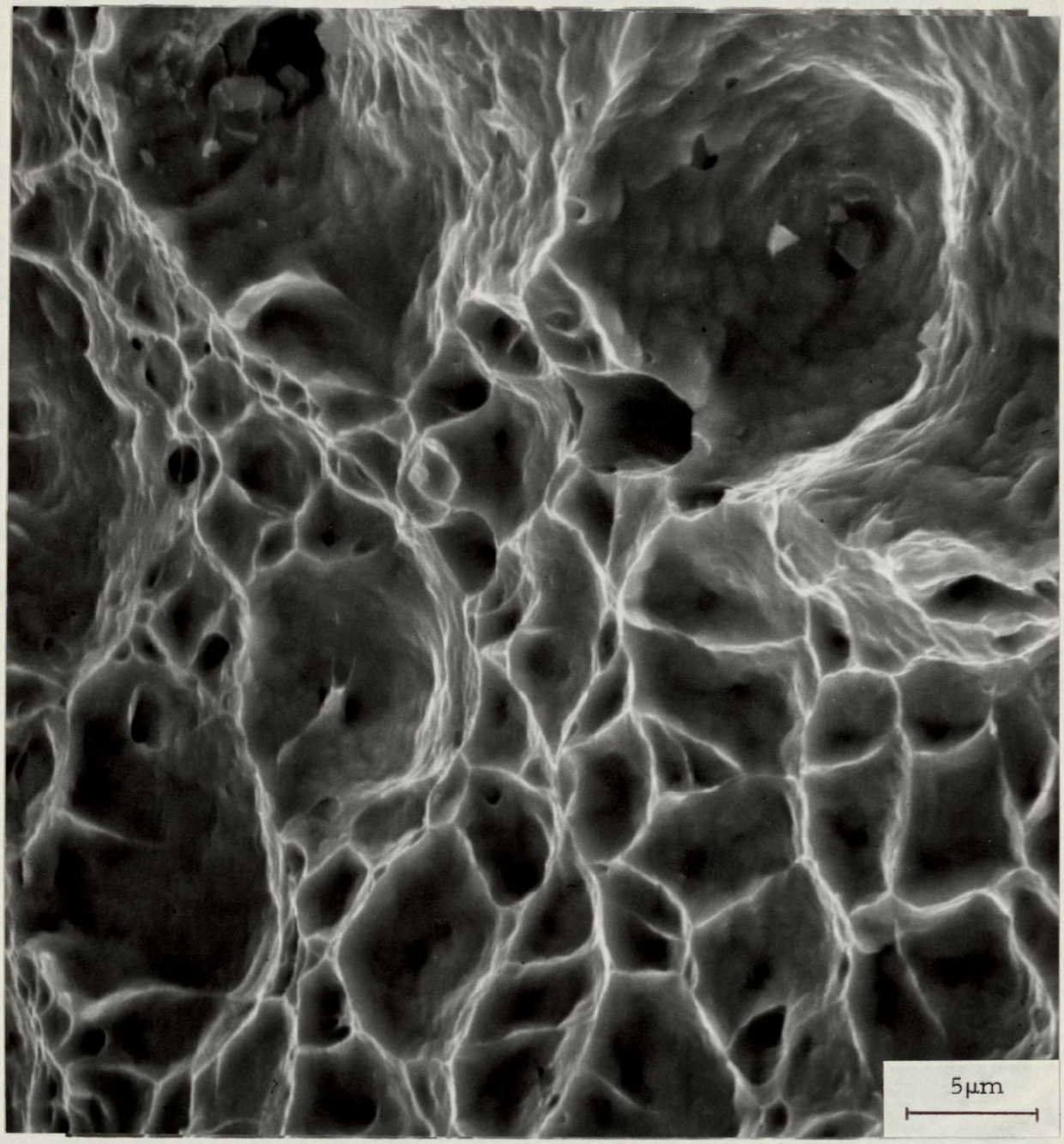

Figure 12 SEM fractograph of the solution treated, 718 MN/m^2 (104 ksi) yield strength tensile specimen fracture.

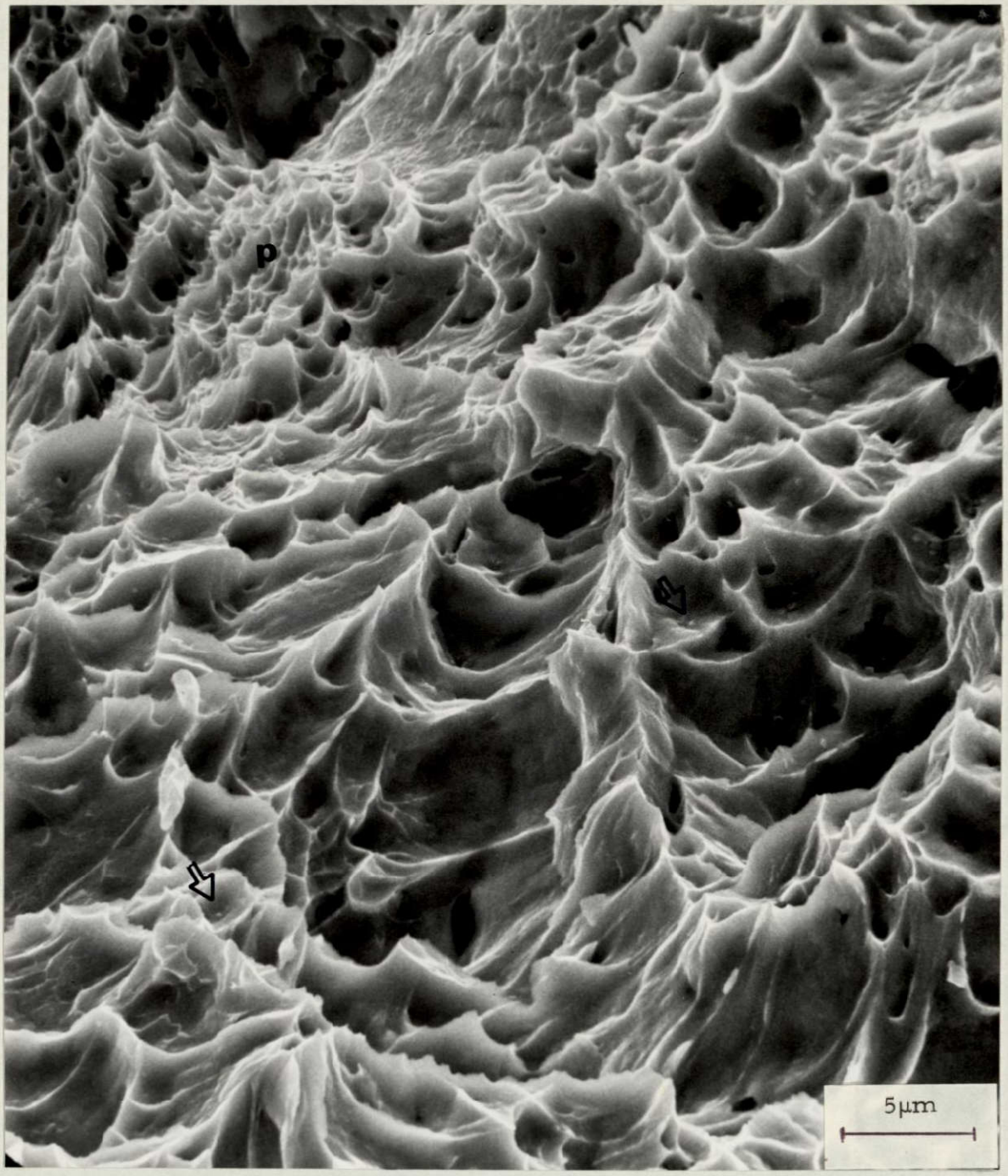

Figure 13 SEM fractograph of the fully aged, 2070 MN/m^2 (300 ksi) yield strength tensile specimen fracture. (The strengthening precipitate dimples are marked "p." Arrows mark the TiC inclusions that are resolved).

Figure 14 TEM replica fractograph from a K_{Ic} fracture of the 2070 MN/m^2 (300 ksi) yield strength condition. (Impressions of nucleation sites the size of strengthening precipitates are indicated by arrows).

TABLE IV

Quantitative Fractography of the Ti(C, N)-Ti_2S, TiC, and Precipitate Dimples Observed on 18 Ni, 300 Grade Maraging Steel Specimens Tested at Room Temperature

(Mean ± Std. Dev.)

Feature	Yield Strength											
	Solution Treated 104 ksi		209 ksi		225 ksi		Commercial Aged 269 ksi		Overaged 246 ksi		Fully Aged 300 ksi	
	Tensile	K_{Ic}	Tensile	K_{Ic}	Tensile	K_{Ic}	Tensile	K_{Ic}	Tensile	K_{Ic}	Tensile	K_{Ic}
Areal Fraction Covered by Large Dimples (Ti(C, N)-Ti_2S) (%)	41.9±12.6	-	37.2±7.9	36.9±7.5	33.8±9.8	33.0±8.8	33.6±6.4	33.1±6.0	23.0±10.2	23.4±8.0	17.6±9.5	16.9±7.0
Areal Fraction TiC Dimples (%)	58.1±12.6	-	62.8±7.7	63.1±7.0	66.2±9.1	67.0±8.1	62.9±7.6	63.0±6.8	51.2±9.8	52.2±7.7	63.5±8.3	63.0±9.1
Areal Fraction Precipitate Dimples (%)	None	-	None	None	None	None	3.5±2.2	3.9±2.0	25.8±3.4	24.4±3.9	18.9±9.75	20.1±6.9
Minimum Diameter TiC Particle Impression (μm)	0.25±0.05	-	0.18±0.03	0.20±0.05	0.15±0.04	0.17±0.05	0.09±0.03	0.10±0.04	0.08±0.01	0.08±0.03	0.06±0.03	0.07±0.02
Average Diameter Precipitate Dimple (μm)	None	-	None	None	None	None	0.10±0.02	0.09±0.01	0.07±0.01	0.07±0.01	0.10±0.01	0.09±0.02
Average Diameter (Ti(C, N)-Ti_2S) Dimples (μm)	22.0±9.9	-	11.5±5.5	11.8±5.1	11.8±4.7	11.0±4.0	11.4±4.1	10.9±3.6	10.8±5.5	10.6±5.0	9.4±2.4	9.0±2.0
Average Diameter TiC Dimples (μm)	4.0±2.2	-	3.7±1.7	3.9±1.1	3.1±1.4	3.2±1.7	2.8±1.3	2.7±1.1	2.6±1.0	2.5±1.2	2.2±1.1	2.1±0.7
Number (Ti(C, N)-Ti_2S) Dimples Per Unit Area ($10^3/mm^2$)	1.7±0.4	-	3.3±0.8	3.0±0.9	2.7±0.3	2.5±0.2	1.7±0.5	1.8±0.6	1.6±0.3	1.8±0.2	2.1±0.8	1.9±0.8
Number TiC Dimples Per Unit Area ($10^3/mm^2$)	32.9±14.0	-	49.1±7.1	49.0±7.5	64.4±7.4	65.0±6.1	81.0±9.8	82.7±8.0	74.5±16.2	75.3±9.2	111.6±18.4	114.1±10.3

ous strength levels appear to be in the amount and size of TiC and precipitate nucleated dimples. Although this may or may not appear to be adequate evidence with which to work out a fracture mechanism, more than after-the-fact fractographic information would seem essential. Irregardless of the fracture surface differences, fractography cannot distinguish between these materials as far as the timing of the void initiation, growth, and coalescence events are concerned. Variously strained and sectioned tensile specimens can provide a direct means by which to measure the influence of microstructure and determine why the most ductile material can tolerate a strain of 1.5 before failure while the least tough material fractures at a strain of only 0.4.

To justify the sectioned tensile technique, similarity between the K_{Ic} and tensile specimen fractures at each strength level is essential. Table IV gives the average and standard deviation of the quantitative fractography data on the Ti(C, N) + Ti_2S, TiC, and precipitate dimples (when they are present). The large (Ti(C, N) + Ti_2S) inclusion nucleated dimples were grouped together due to the difficulty in distinguishing between the Ti(C, N) and Ti_2S fragments at the bottoms of the large dimples. The standard deviation of the areal fraction and number per unit area data were calculated from the average measurements on each of the six fractographs. The standard deviations of the dimple diameters for each type dimple were calculated from the data of the individually measured dimples. Although the standard deviations of the areal fraction and number per unit area

The minimum size TiC inclusion found on the fracture surface decreases as the strength increases, as shown in Table IV. Relative to the Ti(C, N) or Ti_2S, with the high volume fraction of TiC inclusions in such a strong matrix, it is not too surprising that the fracture process is so significantly controlled by the 1 μm or less TiC inclusions. In all conditions considered, the areal fraction of TiC nucleated dimples is nearly 60% of the fracture surface area.

Once sufficient stress levels are attained (higher strength material) the strengthening precipitates, which are about an order of magnitude smaller than the TiC inclusions, are active in the fracture process. Unlike the Ti(C, N), Ti_2S, or TiC inclusions, the strengthening precipitates represent a distribution of particles which are not independent of material strength level. The strengthening precipitates change in size and overall character with degree of aging which, in turn, dictates the strength and flow properties of the material. The extent of growth and loss of coherency of the strengthening precipitates determines whether or not these particles will become active sites for void formation. In the 1856 and 2070 MN/m^2 (269 and 300 ksi) yield strength materials, some of the precipitates in both of these conditions apparently are subjected to stresses which are adequate to cause voids to form at some point in the fracture process. Overaging at 538°C (1000°F) for 3 hours coarsens the precipitates which results in a strength loss to 1697 MN/m^2 (246 ksi). Even at the lower strength, however, the precipitates are sufficiently large and inco-

data are quite large, it appears that the fracture surfaces of the tensile and K_{Ic} specimens for all conditions are statistically identical. Much of the scatter in data can be explained by the non-uniform distribution of the various type inclusions in the material as is evidenced by the quantitative metallography data in Table II.

As the strength level is increased, the major changes in the fracture surfaces are the number of TiC nucleated dimples per unit area and the dimple size. Further, as the strength increases and/or ductility decreases, the decrease in the areal fraction covered by Ti(C, N) or Ti_2S nucleated dimples is taken up by an increase in the areal fraction of TiC dimples coupled with the presence of precipitate nucleated dimples in the three highest strength levels. The solution treated material which is the toughest fracture has the fewest TiC nucleated dimples while the 2070 MN/m^2 (300 ksi) yield strength material, which has the lowest K_{Ic}, contains the largest number of TiC nucleated dimples per unit area. On the average, the solution treated and fully aged tensile fractures have 32.9 and 111.6 thousand TiC dimples per square millimeter, respectively. The number per unit area of TiC nucleated dimples increases continuously as the yield strength increases due to a broader portion of the TiC particle size distribution, including smaller and smaller TiC inclusions, which form voids. With the interparticle spacing between the critical size TiC inclusions decreasing, the dimple size decreases since less growth is needed to get impingement of nearest neighbor voids.

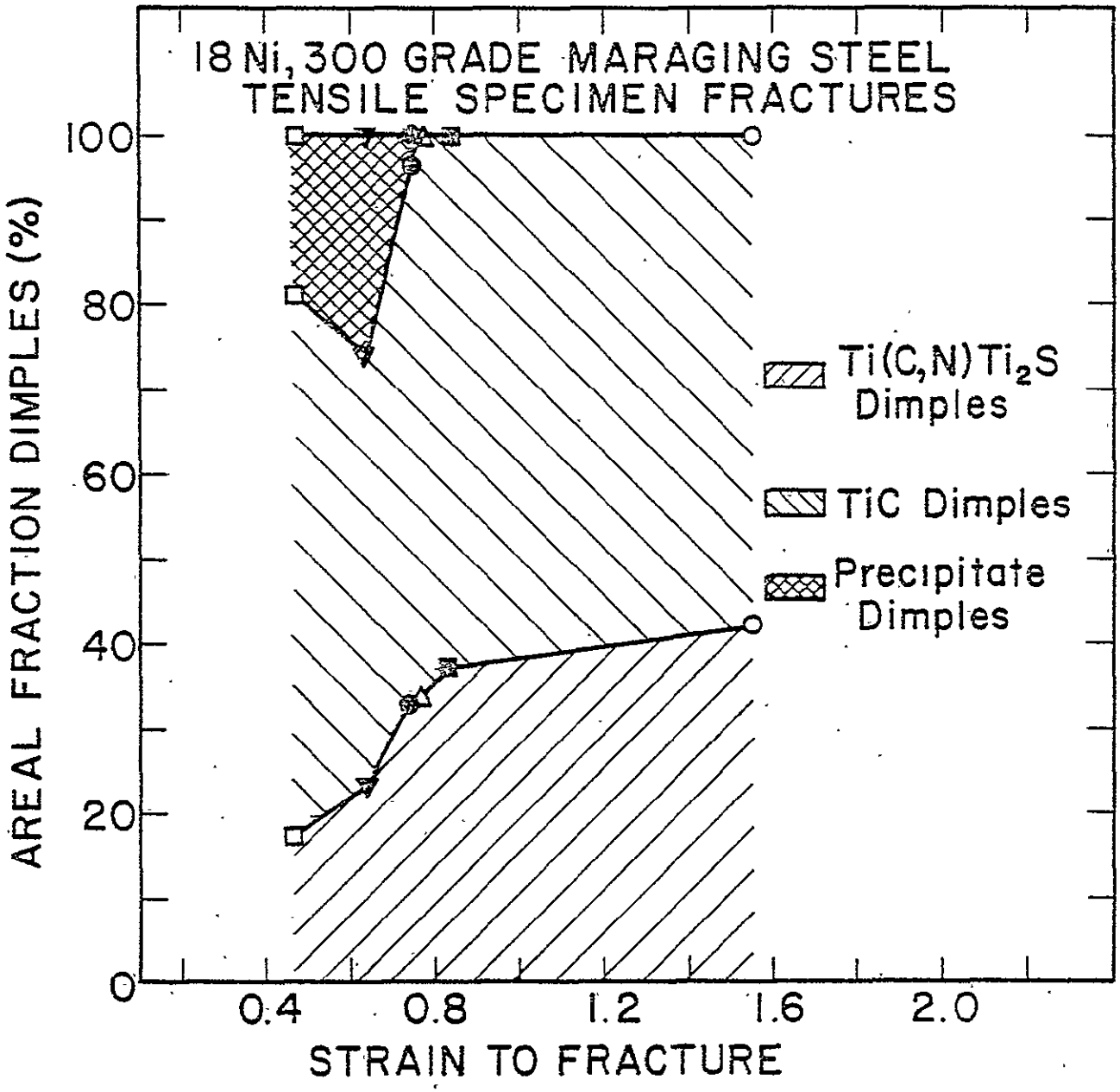

Figure 15 Variation with strain to fracture (toughness) in the areal fractions of Ti(C,N)-Ti_2S, TiC, and precipitate nucleated dimples covering tensile specimen fractures.

herent to become sites for voids. With the effect of particle coarsening more significant than strength loss, the ductility or toughness is much lower than the underaged material of similar yield strength.

The relative areal fractions of Ti(C, N) or Ti_2S inclusion, TiC inclusion, and possibly Ni_3Mo or Fe_2Mo precipitate nucleated dimples which make up the fracture surfaces at specific strength levels have been plotted against fracture strain in Figure 15. The various regions in this plot account for the ductility loss in terms of the relative importance of the various inclusion and strengthening precipitate dimples. Up until the 1553 MN/m^2 (225 ksi) yield strength level, only a slight increase in the areal fraction of TiC dimples occurs. How then might the loss in fracture strain from 1.5 to 0.8 be explained? Although about the same portion of the fracture surface is covered by Ti(C, N)-Ti_2S and TiC nucleated dimples, in the stronger (less ductile) condition the dimples are much smaller and, in turn, greater in number to cover the same area. Only the sectioning studies can supply the necessary information as to the strain (timing) at which various voids (dimples) form, the rate at which they grow, and the mechanism by which they coalesce. In the three strongest (least tough) conditions and particularly in the overaged material, the strengthening precipitate nucleated dimples serve to suppress the Ti(C, N)-Ti_2S and TiC dimple activity (growth). In the high strength cases, the formation of voids at precipitates apparently speeds up the fracture process. The sectioned ten-

bered that the void initiation, growth, and coalescence events do not happen just at discrete times in the process but rather occur simultaneously after the first voids are formed. Independent of strength level, in the 300 grade maraging steel the first voids to form were invariably nucleated at the large second-phase Ti(C, N) and Ti_2S inclusions. With additional straining, the existing voids grow while additional voids are nucleated at smaller Ti(C, N) and Ti_2S inclusions. While void nucleation occurs at Ti (C, N) and Ti_2S inclusions, as stress and strain levels increase, voids grow in this material by the formation of fine cracks which emanate from the large voids along a path of critical size TiC inclusions. This unique crack branching along a path of TiC inclusions occurs by a repetition of ductile tearing of the matrix and separation at the TiC inclusion-matrix interface. As can be seen, the fracture process occurs by a complex sequence of void nucleation and growth which is anything but discrete. If stresses of sufficient magnitude are attained and precipitates are large enough, rapid separation at these extremely fine particles occurs by localized nucleation events which make up the void coalescence process.

The details of the mechanism of void nucleation at the Ti(C, N) and Ti_2S inclusions and the unusual way the voids grow in a branched path along the fine TiC inclusions will be given in the following sequence of micrographs. The events leading to fracture in this material are very similar at all yield strength levels. The level of stress, strain

sile studies will further account microstructurally for the loss in ductility from a fracture strain of 0.8 to nearly 0.4.

SECTIONED TENSILE STUDIES

It is impossible from fractography alone to determine how the microstructure is participating in the fracture event as a function of strength. Although the fracture surfaces are somewhat similar over a wide range in yield strengths, it has been demonstrated that the strongest material can accommodate less than one-third the strain that the unaged material can before failure. Through sectioning, differences in the timing or rate at which voids form, grow, and coalesce at different strength levels can be distinguished. A series of tensile specimens from each yield strength material were deformed at room temperature to various strains up to and including that required for fracture. These specimens were sectioned to their midplanes on a plane parallel to the plate surface and prepared for metallographic observation. In conditions beyond necking, only the necked regions were studied. The optical microscope and SEM were used to characterize the fracture process.

Progress of Fracture

Fracture in the 18 Ni, 300 grade maraging steel occurs in stages of void nucleation, growth, and coalescence. In many ways, this mechanism is similar to the classical dimpled rupture in aluminum alloys[20] and steels.[3] It must be remem-

inclusion cracking. Failure of a large Ti(C, N) inclusion in the 2070 MN/m^2 (300 ksi) material is shown in Figure 17. This particular inclusion has cracked in several places leaving fragments of the particle in the center of the void. There are, however, a significant number of cases where the Ti(C, N) inclusions have separated from the matrix. Most often the particle failure occurs by a combination of these two mechanisms. Independent of the material yield strength the first voids that form are nucleated at the largest Ti(C, N) or Ti_2S inclusions in the material. As deformation proceeds, the first voids to form continue to grow while additional voids are nucleated at smaller and smaller inclusions that exist in the size distribution of inclusions described by Figure 9.

The void growth process in the 300 grade maraging steel at all strength levels considered occurs by a repetitive sequence comprised of void nucleation at a TiC inclusion followed by ductile tearing to an adjacent critical size TiC inclusion and so forth. The main (Ti(C, N) or Ti_2S) void tends to elongate in the tensile direction while the TiC nucleated voids emanate as many cracks from the central cavity. The unique way in which the fine cracks propagate along the TiC inclusions is shown in Figure 18. Notice the depression in the matrix marked with an "X" in Figure 18. Continued polishing of similar voids by serial sectioning has indicated that a large Ti(C, N) or Ti_2S inclusion nucleated void exists below the indentation from which the TiC nucleated voids extend and encircle the main void. Once the

and overall rate of void initiation and growth varies significantly with strength. These differences will be explained in the quantitative sectioned tensile data given below.

At all strength levels given in Table III, void initiation at either Ti(C, N) or Ti_2S inclusions does not occur before a small yet measurable amount of plastic deformation. Metallographic examination of the as-received forged plate has indicated in Table II that roughly 5 and 19% by volume of the Ti(C, N) and Ti_2S inclusions, respectively, are precracked due to the forging operation. Independent of matrix strength, however, the Ti(C, N) and Ti_2S inclusions usually fail by a combination of particle cracking and particle-matrix interface separation. At a strain of 0.014, an early stage in the deformation process of the 718 MN/m^2 (104 ksi) material, Figure 16 shows void nucleation at an irregular shaped Ti_2S inclusion. From this evidence and other micrographs (not shown), it appears that the Ti_2S inclusions usually fail by separation at the particle-matrix interface. Although the Ti_2S inclusions are much softer than the very brittle Ti(C, N) inclusions, they are usually so irregular that they frequently break up into many fragments. After extensive straining, some Ti(C, N) inclusions crack while others fail by particle-matrix interface decohesion. In the fully strengthened 2070 MN/m^2 (300 ksi) material, a similar situation exists. In this condition at equivalent strains, the stresses are much higher and it appears that the Ti(C, N) inclusions fail more frequently by

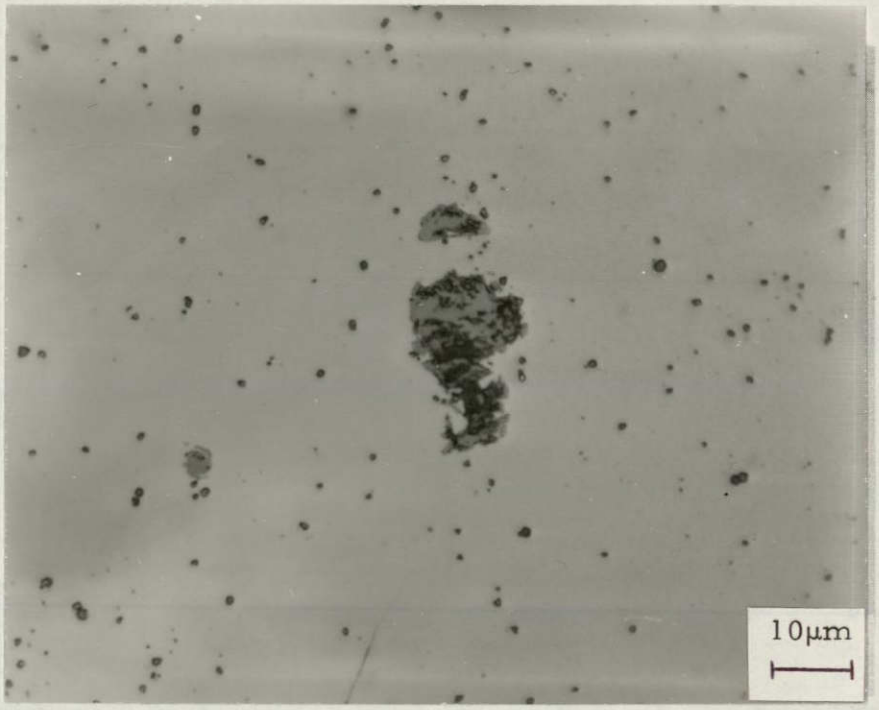

Figure 16 Optical micrograph of a sectioned tensile specimen of the 718 MN/m^2 (104 ksi) material strained to 0.014. The tensile axis is vertical.

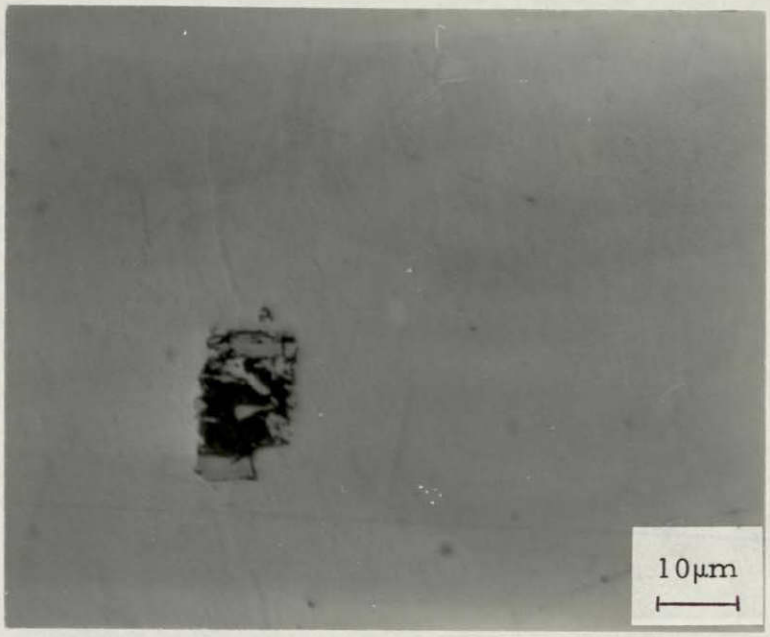

Figure 17 Optical micrograph from a sectioned tensile specimen of the 2070 MN/m^2 (300 ksi) material strained to 0.487. Tensile axis is vertical.

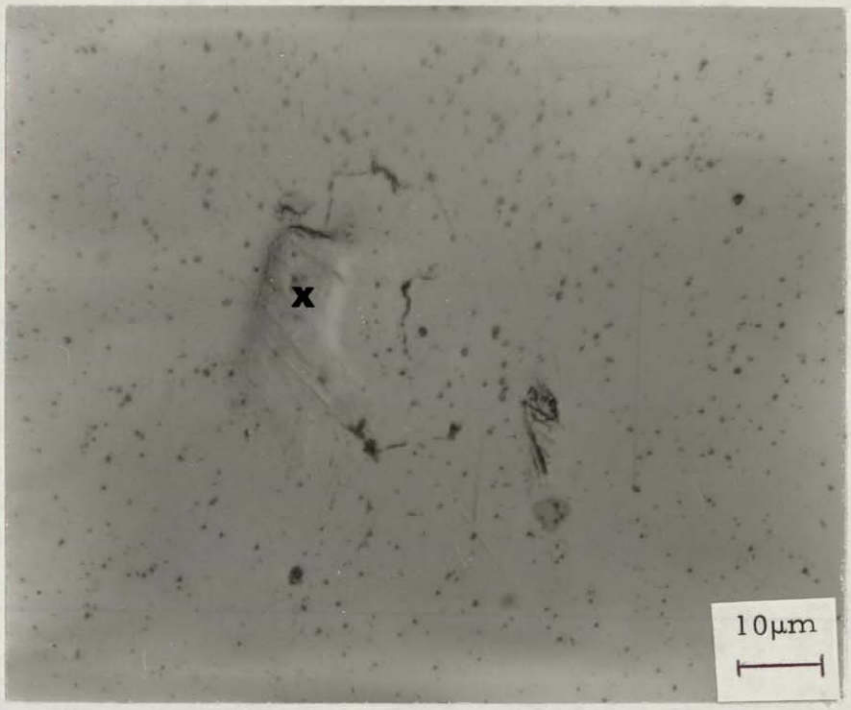

Figure 18 Optical micrograph of a sectioned tensile specimen of the 718 MN/m^2 (104 ksi) material strained to 1.550. The depression in the matrix is marked with an "x." The tensile axis is vertical.

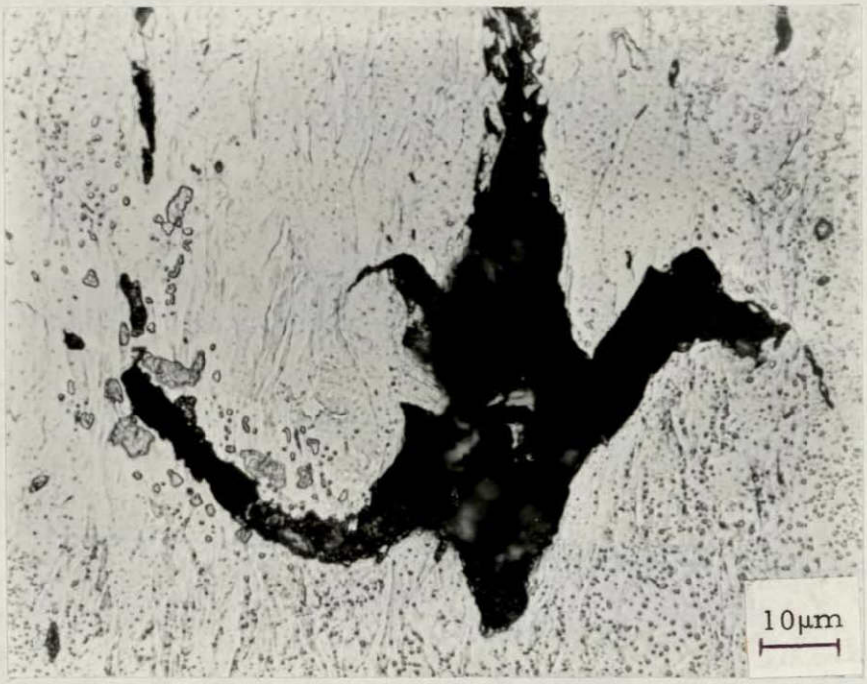

Figure 19 Optical micrograph of a sectioned tensile specimen of the 718 MN/m^2 (104 ksi) material strained to 1.550. The tensile axis is vertical.

sile specimen can tolerate short of fracturing. At about one-third the level of strain accommodated by the unaged material, the fully aged material has a much larger number of voids present within the specimen section. All of the large Ti(C, N) and Ti_2S inclusions which have formed voids in the unaged material are voided in this condition. In addition, most of the small inclusions from the fine diameter end of the Ti(C, N) and Ti_2S inclusion size distributions have nucleated voids. Because the 2070 MN/m^2 (300 ksi) yield strength material does not readily deform, void growth is severely suppressed. This can be seen when the void in the 2070 MN/m^2 (300 ksi) material (Figure 20) is compared to the micrograph (Figure 19) of the 718 MN/m^2 (104 ksi) solution treated material which was taken at equivalent magnification. There are many more including smaller Ti(C, N), Ti_2S, and particularly TiC inclusions that form voids in the fully strengthened material. Thus the interparticle spacing between nearest neighbor critical size TiC inclusions is reduced (Table IV) and hence far less growth at each void site is necessary to cause failure. The decrease in dimple size follows directly from the reduction in the spacing between void nucleating inclusions. The original void nucleation site in Figure 20 was the fractured Ti(C, N) inclusion which has been marked by an arrow.

After many voids have grown in a relatively stable manner to a complex shape similar to that in Figure 19, void coalescence in the 718 MN/m^2 (104 ksi) material occurs by ductile tearing between these large voids by void nuclea-

fracture strain is reached, much of the void nucleation site information is obscured by extensive deformation and large voids. It is clear, however, that the solution treated material can tolerate extremely large voids which originate at large Ti(C, N) or Ti_2S inclusions and grow in an irregular fashion along many neighboring fine TiC inclusions. Relative to the 2070 MN/m^2 (300 ksi) material, voids grow in the 718 MN/m^2 material in a very stable fashion. This results in large voids comprised of at least one Ti(C, N) or Ti_2S void and many interconnecting TiC nucleated voids. Final tensile section separation occurs by link up of voids similar to the one shown in Figure 19.

The fully aged material can only accommodate a plastic strain of 0.468 before fracture. The 2070 MN/m^2 (300 ksi) yield strength tensile specimen shows the least amount of necking of all materials examined. This condition also results in the most rapid sequence for void nucleation, growth, and coalescence in the 18 Ni, 300 grade maraging steel. After straining to 0.298, the fully strengthened material has exhausted more than half of the plastic strain that it can withstand before failure. At this level of strain, very little void activity has taken place in the 1553 MN/m^2 (225 ksi) material; and in the 718 MN/m^2 (104 ksi) unaged material, an additional strain of more than 1.25 can be accommodated before unstable fracture. The similarity in the mechanism of void initiation and growth is apparent in Figure 20. Strained plastically to a level of 0.487, Figure 20 represents the most deformation that the 2070 MN/m^2 (300 ksi) ten-

Figure 20 Optical micrograph of a sectioned tensile specimen of the 2070 MN/m^2 (300 ksi) material strained to 0.487. The Ti(C,N) inclusion nucleation site is marked by an arrow. The tensile axis is vertical.

tion at additional TiC inclusions that are about 0.1 μm in diameter. In all of the low strength conditions in the 300 grade maraging steel, the coalescence process might be thought of as occurring by the impingement of nearest neighbor TiC inclusion nucleated crack branches. In the three highest strength materials in Table III, void coalescence occurs by a combination of TiC void nucleation and growth, and by catastrophic separation at strengthening precipitates which serve to prematurely terminate the void growth process. Careful examination of the submicron size dimples on these fractures with stereo pairs has provided the key information necessary to correlate the fracture topography to the microstructure.

The overaged material has a yield strength of 1697 MN/m^2 (246 ksi) which is lower than that for the commercially aged material which is 1856 MN/m^2 (269 ksi). Although the overaged material has lower strength, it is also less ductile or tough. This apparent inconsistency results from the more significant influence of the coarsened strengthening precipitates which serve to abort the deformation process at a lower plastic strain than in the stronger material. In an underaged material at a yield strength equivalent to the overaged material, it follows that with the same Ti(C, N), Ti_2S and TiC inclusions present, similar void nucleation and growth would occur. The difference arises in that in the overaged material the strengthening precipitates assist in the void coalescence process to significantly reduce the strain to fracture.

Void coalescence is confined mainly to the unstable portion of fracture. This is supported by the areal fraction of fine dimples on both high and low yield strength tensile specimen fracture surfaces. It has already been indicated that a similarity exists in the growth and coalescence processes occurring at TiC inclusion crack branching in both low and high strength conditions. The additional contribution of precipitates to the coalescence of voids is the subject of further investigation. Because of the experimental difficulty in directly observing the coalescence process, evidence from several techniques were used to demonstrate the difference in the coalescence mechanism in the high strength conditions.

In the commercially aged, 1856 MN/m^2 (269 ksi); the fully aged, 2070 MN/m^2 (300 ksi); and overaged 1697 MN/m^2 (246 ksi) yield strength conditions, the strengthening precipitates become very effective barriers to slip. The strengthening precipitates are from 200 to 500 Å (0.02-0.05 μm) in diameter in the commercial and fully aged conditions. In the overaged material, the precipitate particles have coarsened to nearly 1000 Å (0.1 μm). While these particles serve to block dislocation movement, the stress concentrations at these sites are extremely intense. The combination of precipitate size, density, and resulting stress concentration in the matrix ligament between nearest neighbor TiC cracks is sufficient to produce slip offsets in the martensite laths. The optical micrograph of the 2070 MN/m^2 (300 ksi) yield strength tensile specimen strained to a level of

0.402, sectioned, and etched shows many intersecting slip traces in Figure 21. None of these markings were present on any of the materials before plastic deformation. Similar intense slip traces were revealed on the 1856 and 1697 MN/m^2 (269 and 246 ksi) yield strength materials. No evidence of slip offsets were seen on any of the lower strength materials at any level of deformation. Clearly shown in the center of Figure 21 is a martensite lath with several offsets along the boundaries which have occurred due to intense localized shear. The precipitates that lie along these shear bands running across the width of the martensite laths are subject to stress and strain concentrations that are far in excess of the average tensile stress and strain values.

To be certain that the deformation markings on deformed, polished, and then etched tensile specimens were due to slip, several plane-strain tensile specimens were prepared. The flat sheet samples were similar in design to those used by Clausing.[21] After these specimens were aged, electropolished and deformed, the surfaces subject to plane-strain were viewed directly in the SEM. The intense shear bands and lath offsets in the three highest strength materials were confirmed by this technique.

TEM thin-foils were cut from the neck of a fractured, 2070 MN/m^2 (300 ksi) yield strength round tensile specimen. The amount of deformation made direct observation of slip steps difficult due to the high dislocation density present at these levels of stress and strain. The proof that the

laths were sheared late in the deformation process in the high strength material is shown in Figure 22. Although some instances of fine cracks traversing the width of laths were observed, evidence would not be clear enough to hold up under careful scrutiny. Clearly, however, one can see where the localized strains caused by intense shear offsets lead to a much higher local strain concentration than is macroscopically measured as plastic tensile strain. Once final ligament separation occurs, the fracture surface trace should contain extremely fine dimples which can be associated with the voids formed at precipitates. Adjacent to the precipitate nucleated dimples should be the larger TiC voids (dimples) that were joined by the sheet of precipitate dimples. The SEM fractograph of the 2070 MN/m^2 (300 ksi) yield strength tensile fracture shows a direct correlation to the mechanism of coalescence at extremely fine strengthening precipitates. The density of shallow dimples in the center of the fractograph in Figure 23 is clearly related to the precipitates that are spaced only a few hundred angstroms apart. The width of the fine dimpled region is about 10 μm which is also in excellent agreement with the width of the martensite laths.

Quantitative Sectioning Studies

To fully understand the influence of strength on fracture toughness, at each yield strength level the void initiation, growth, and coalescence stages of fracture were described in a more quantitative manner. The central re-

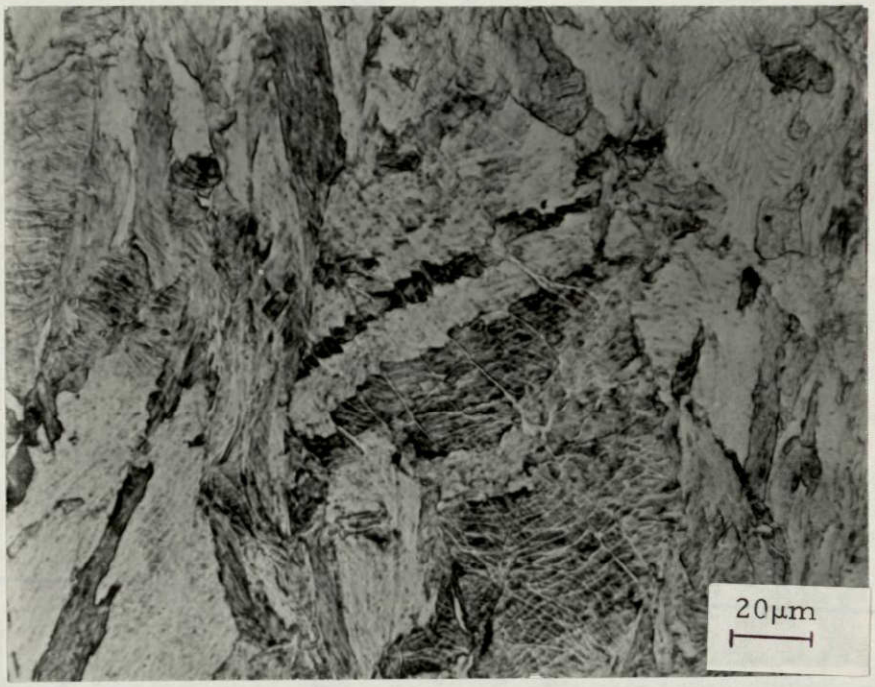

Figure 21 Optical micrograph of a 2070 MN/m^2 (300 ksi) yield strength tensile specimen strained to a level of 0.402, sectioned, and etched showing many intersecting slip traces. The tensile axis is vertical.

Figure 22 TEM micrograph of a thin-foil taken from the necked region of a fractured tensile specimen of the 2070 MN/m^2 (300 ksi) yield strength material. The shear bands and lath boundary offsets created are marked by arrows. The ledge of dimples in Figure 23 corresponds to region "L."

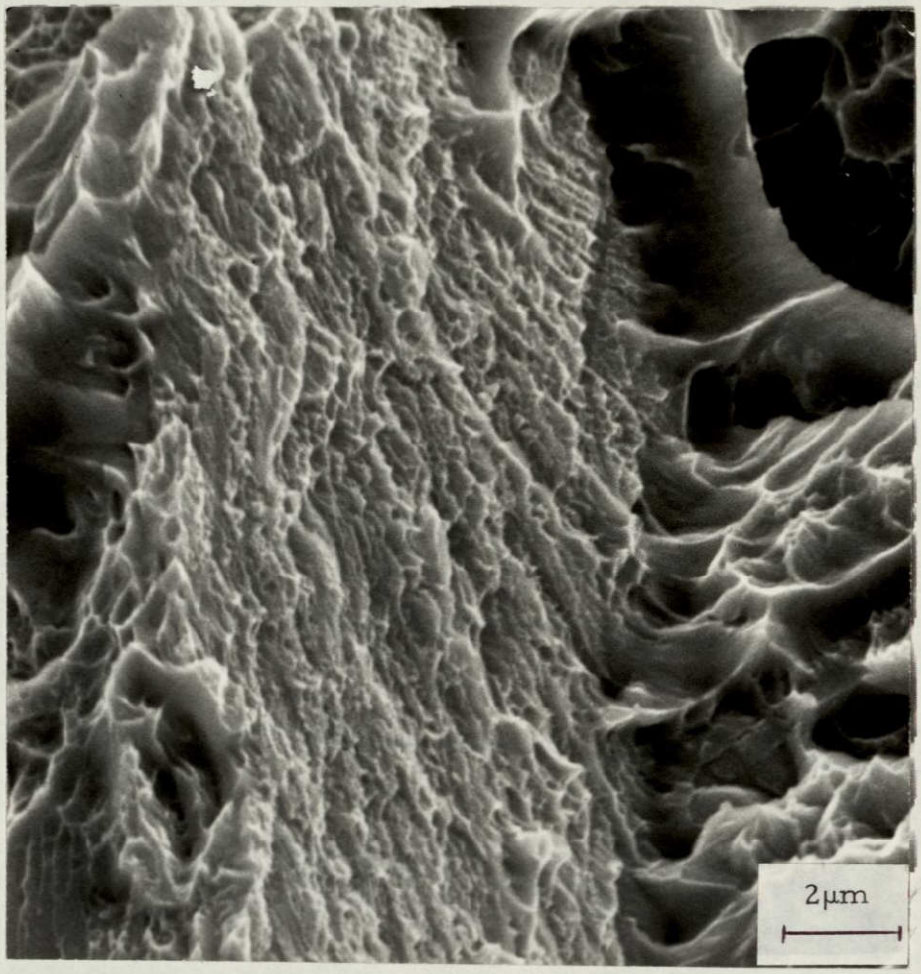

Figure 23 SEM fractograph of the 2070 MN/m^2 (300 ksi) yield strength tensile fracture showing a ledge of extremely fine precipitate nucleated dimples. The ledge surface corresponds to the sheared region in the interior of a lath similar to the area marked "L" in Figure 22.

gion at the longitudinal midplane in tensile specimens 2.23 mm (0.088 in.) wide and 2.5 mm (0.10 in.) in the axial direction was studied using quantitative metallography. This sampling area was chosen to avoid the shear lip regions in the 6 mm (0.25 in.) diameter smooth, round tensile specimens. At all strength levels studied, the region where most voids formed was roughly equivalent. Since a constant specimen geometry was used, the same area was centered in the necked tensile specimens. At a magnification of 1000x, these dimensions were translated to 160 fields-of-view characterized quantitatively using an optical microscope. To document the effect of yield strength on the timing of the nucleation, growth, and coalescence of voids (ductility or toughness), for each material and degree of deformation, the number, source, size, and percent of inclusions with voids were measured.

In each of the yield strength conditions, the void nucleation and growth sequence leads to a large inclusion nucleated void encircled by branches or tentacles of TiC inclusion nucleated "cracks." An example of Ti(C, N) void nucleation and growth by branching along a path of TiC inclusions was shown in the optical micrograph of the 718 MN/m^2 (104 ksi) yield strength tensile specimen in Figure 18. This figure is representative of the unique void shape that is formed due to the sequence of void nucleation and growth in this system. The fractographic results have already indicated that the TiC nucleated dimples occupy more than 50% of the fracture surface in all strength levels con-

sidered. With this consideration along with the indicated shape of the voids in the sectioned tensiles, it would appear that measurements of void area directly from the sectioned plane would not be representative of the voids or dimples which ultimately make up the fracture surface. A series of low and high strength tensile specimens were serially sectioned to more systematically determine the three-dimensional shape of the branched voids. These sections also provide conclusive evidence that a large void of roughly spherical shape nucleated at a Ti(C, N) or Ti_2S was, in all cases, the center from which TiC nucleated branches propagated.

Since the sectioning plane represents only a single cut (or line profile) through a surface of many TiC voids or dimples, the measurement of TiC nucleated crack length on the sectioning plane must be properly corrected for the shape difference revealed in the normal plane. The results of void shape measurements from several sectioned voids has indicated that the crack branch can be approximated as an ellipse that is about 1.2 times as long as it is wide. The Ti(C, N) and Ti_2S inclusion nucleated voids are no problem since they are considered spherical. To determine area of the normal or fracture plane occupied by Ti(C, N) or Ti_2S nucleated voids, the diameter of each void observed on a sectioning plane was converted to the area of a circle of this diameter and the individual areas summed over the entire section. Each TiC nucleated branch was measured and this length of the ellipse was multiplied by the proper

width to get the normal plane area. Areas from all such branches were added for each sectioned specimen.

Void Initiation

In the 718 MN/m^2 (104 ksi) solution treated material through to and including the 2070 MN/m^2 (300 ksi) fully aged material, the fracture process begins with the nucleation of voids at the largest Ti(C, N) and Ti_2S inclusions that exist in their respective distributions. The frequency of void initiation at Ti(C, N) inclusions is plotted as a function of true plastic strain for the six yield strength conditions shown in Figure 24. The strain axis can be thought of as a time scale. The graph indicates how much strain or analogously how long the tensile specimen will deform before a certain percentage of the Ti(C, N) inclusions have formed voids. Notice that the 2070 MN/m^2 (300 ksi) fully strengthened material can accommodate a strain of only 0.1 before 40% of the Ti(C, N) inclusions present in the sectioning plane have voids associated with them. The 1553 MN/m^2 (225 ksi) material can strain plastically to about 0.5 before 40% of the Ti(C, N) inclusions have voided. The solution treated, 718 MN/m^2 (104 ksi) yield strength material will deform to a strain of 1.55, fracture, and at that point less than 30% of the Ti(C, N) inclusions have participated in the fracture process. Stated in an equivalent manner, after a strain of 0.4 is reached in the 718 MN/m^2 (104 ksi) material, 6% of the Ti(C, N) inclusions have formed voids while 57% are voided in the 2070 MN/m^2

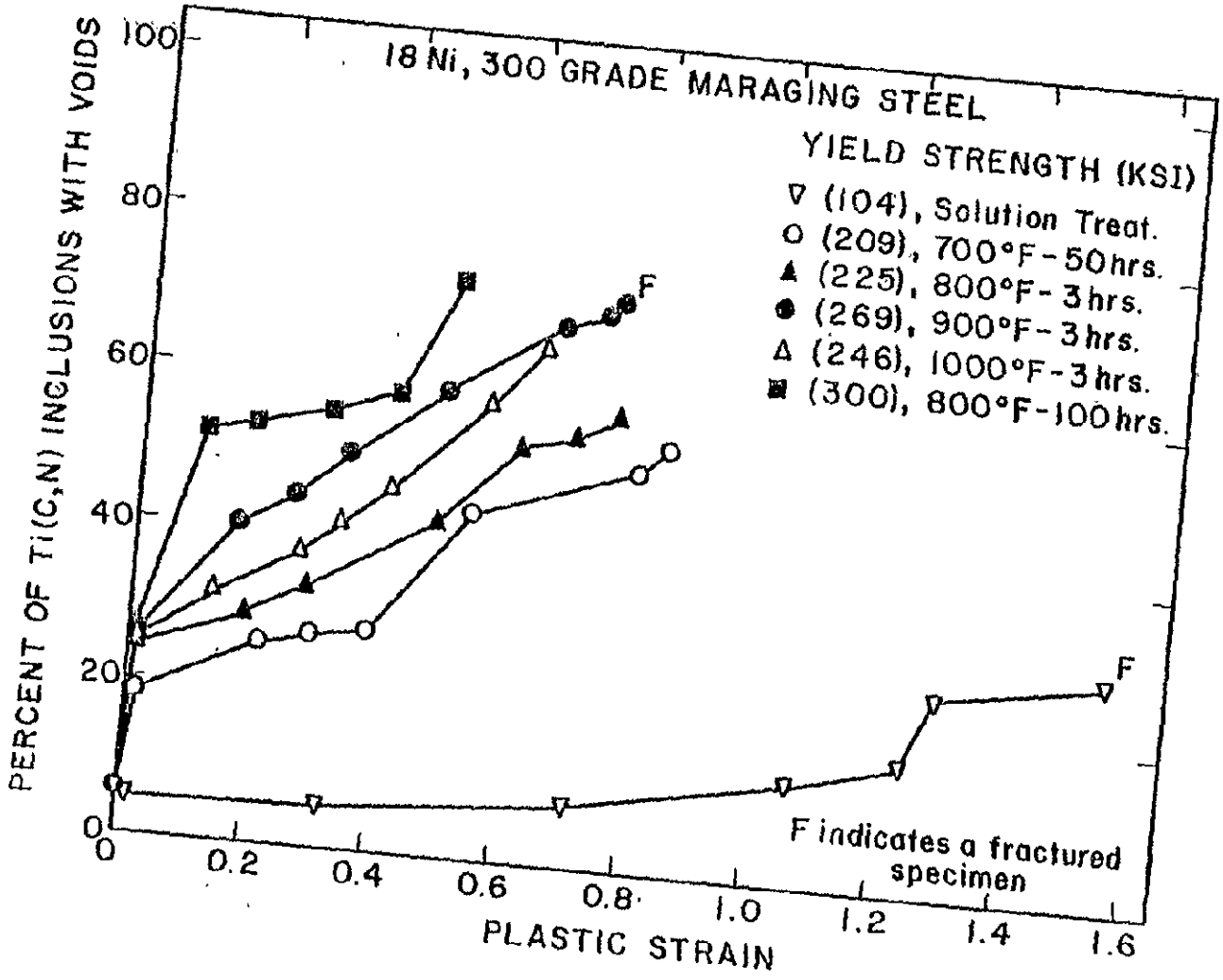

Figure 24 Variation in the frequency of void initiation at Ti(C,N) inclusions as a function of true plastic strain for the various yield strength materials.

(300 ksi) material at the same strain. This condition is related to the significantly higher stress levels that exist in the high versus low strength material at equivalent levels of strain. Also note that the amount of strain that can be tolerated before a certain amount of voids form is proportional to the yield strength. The 1697 MN/m^2 (246 ksi) overaged material can deform with better resistance to Ti(C, N) void formation than the 1856 MN/m^2 (269 ksi) material but not nearly as well as the 1553 MN/m^2 (225 ksi) material. With few exceptions, the largest inclusions fail first and represent the earlier segments of the curves in Figure 24. The 2070 MN/m^2 (300 ksi) material which is the least ductile or tough has the largest fraction of Ti(C, N) inclusions that have nucleated voids in the sectioned tensiles. In the worst case, only 75% of the Ti(C, N) inclusions in the necked area of the sectioned tensile specimen have formed voids. With somewhat less variation between the 1442 MN/m^2 (209 ksi) and 2070 MN/m^2 (300 ksi) materials until after strains of about 0.3, the same tendency exists for void formation at Ti_2S inclusions. The plot of the % of Ti_2S inclusions with voids is similar to the Ti(C, N) plot and is not shown here.

Consideration of the true average applied tensile stresses that are present in the variously aged tensile specimens leads to the plot shown in Figure 25. Nearly independent of the yield strength, once a sufficient level of stress is attained, a percentage of Ti(C, N) inclusions indicated in Figure 25 have nucleated voids. The indica-

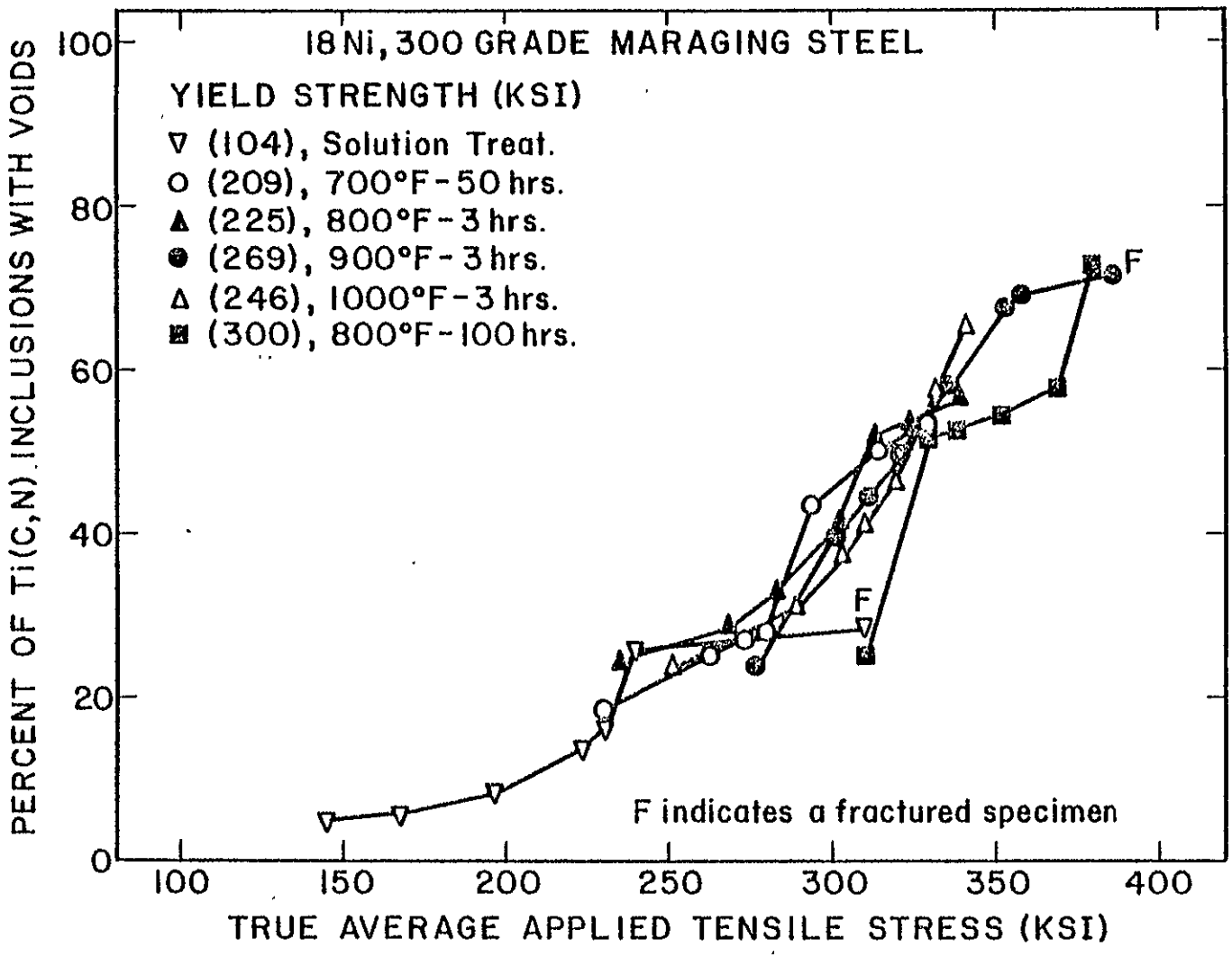

Figure 25 Variation in the frequency of void initiation at Ti(C,N) inclusions as a function of true average applied tensile stress for the various yield strength materials.

tion is that no greater than a certain percentage of Ti(C, N) inclusions will nucleate voids unless stresses greater than a given amount are attained. The process of void formation at Ti(C, N) inclusions is not totally independent of strain, however, since there are significant deviations from a single curve, particularly in the 2070 MN/m^2 (300 ksi) material. The fact that Ti(C, N) inclusions fail most often by a combination of particle cleavage and interface separation is a good indication that the mechanism is both stress and strain dependent. It is interesting to note that even after normalizing the true stress to the fracture stress, by subtracting the appropriate yield stress, or by plotting the Bridgman corrected stress (flow stress), no significant improvement in the trend is attained. In the low strength materials, fewer Ti(C, N) inclusions nucleate voids since the maximum stress levels attained are significantly lower than in the high strength materials.

Figure 26 illustrates the percent of Ti_2S inclusions with voids as a function of true average tensile stress. Within any yield strength material, the percentage of Ti_2S inclusions which form voids increases in a sigmoidal fashion with increasing stress. More so than with the Ti(C, N) inclusions, the Ti_2S particles react differently to the applied stress in the various yield strength materials. In the 718 MN/m^2 (104 ksi) material, 40% of the Ti_2S inclusions are voided after a stress of only 1553 MN/m^2 (225 ksi). The 2070 MN/m^2 (300 ksi) material has already reached a

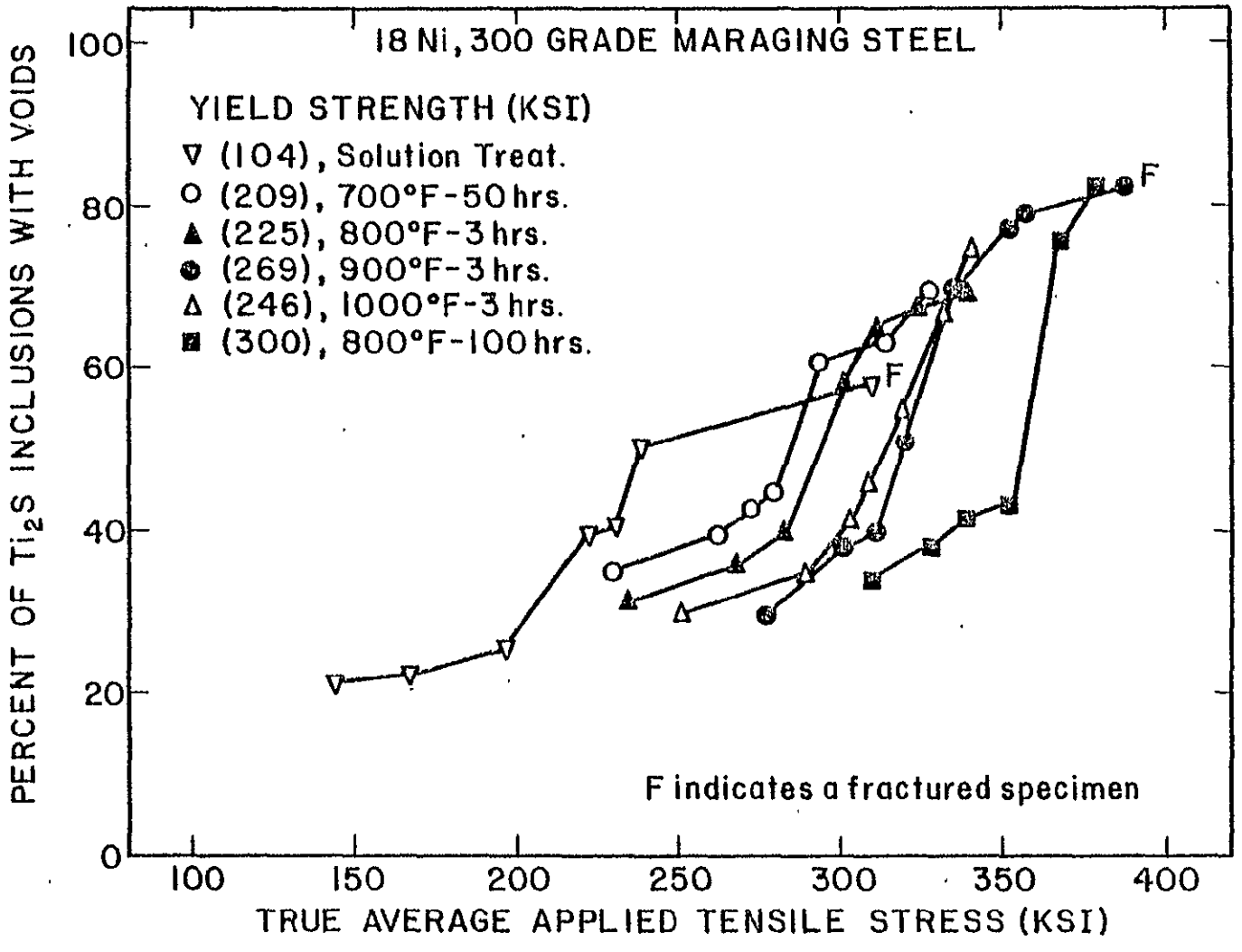

Figure 26 Variation in the frequency of void initiation at Ti_2S inclusions as a function of true average applied tensile stress for the various yield strength materials.

stress of about 2346 MN/m^2 (340 ksi) when 40% of the Ti_2S inclusions are voided. Before 40% of the Ti_2S inclusions have failed, the solution treated material has deformed to a plastic strain of 1.2. The fully aged material, on the other hand, has accommodated a strain of less than 0.2. The strong dependence of Ti_2S void formation on plastic strain is indicated. As with the Ti(C, N) inclusions, the data indicates that a combined stress and strain dependence is operative. The likelihood of an energy dependence for the void initiation frequency is indicated by the combined importance of stress and strain. By integrating the area under the flow curves up to the stress and strain indicated by the data points in any of the above graphs (Figures 24-26), the total energy or work due to deformation up to that strain was considered. This approach unfortunately did not reduce the data to any simple or consistent relationship. It is still thought, however, that void nucleation as a function of yield strength in the 18 Ni, 300 grade maraging steel is controlled by a critical energy to form a void.

Cox and Low[3] have shown that the largest Ti(C, N) inclusions present in an 18 Ni, 200 grade maraging steel are the first particles to fail in the deformation process. Smaller and smaller inclusions that are present initiate voids as the stress due to deformation increases. Van Stone, Merchant, and Low[20] also found that the largest inclusions fail first in several high-strength aluminum alloys. Both of these studies were restricted to deformation

in materials at single strength levels. When each yield strength material is considered separately, the largest Ti(C, N) or Ti_2S inclusions are the first particles to fail with smaller inclusions becoming active void nucleation sites at higher stress levels.

A plot of equivalent inclusion diameter as a function of true average applied tensile stress for all strength levels clearly shows that the critical size inclusion for void nucleation is not solely dependent upon stress. The equivalent particle diameter is the cube edge for the Ti(C, N) and the average of the two dimensions in the plane of normal stress for the ellipsoidal Ti_2S inclusions. Figure 27 shows that before a Ti(C, N) inclusion as small as 3.0 μm nucleates a void, the various strength materials require different stresses. In the 718 MN/m^2 (104 ksi) material, a stress of only about 1380 MN/m^2 (200 ksi) is necessary to initiate a void at a 3.0 μm Ti(C, N) inclusion. A 3.0 μm Ti(C, N) inclusion is free of voids until a stress of nearly 1967 MN/m^2 (2 ksi) in the 1553 MN/m^2 (225 ksi) yield strength tensile specimen. In the fully strengthened material, the 3.0 μm Ti(C, N) inclusions fail on the average only after a stress of 2243 MN/m^2 (325 ksi) is reached. The indication of Figure 27 is that the requirement for void initiation at a certain size Ti(C, N) inclusion is some combination of stress and strain. While a 3.0 μm Ti(C, N) inclusion forms a void in the 718 MN/m^2 (104 ksi) material at about 60% of the stress in the 2070 MN/m^2 (300 ksi) material, the solution treated material has accommoda-

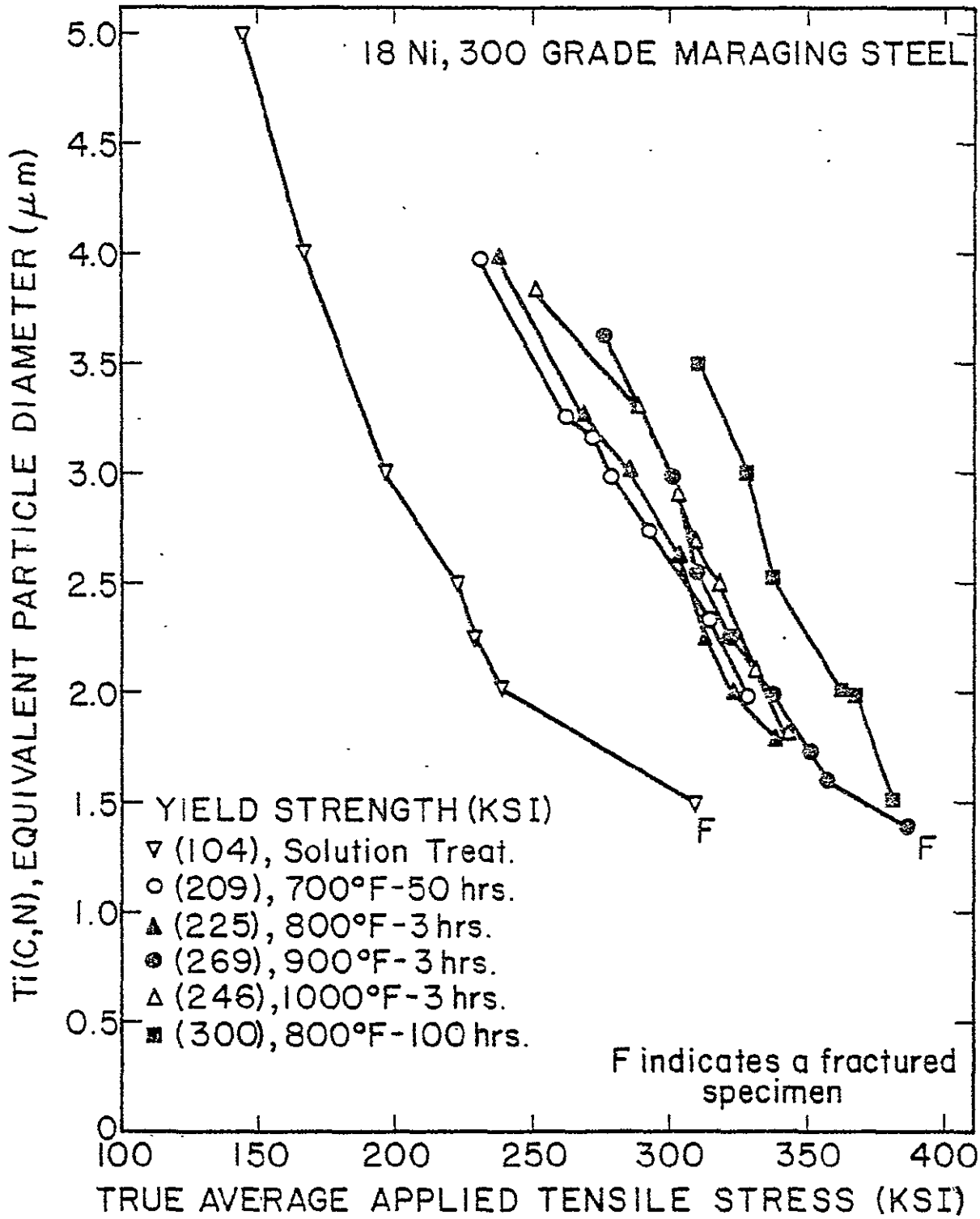

Figure 27 Diameter of the critical size Ti(C,N) inclusion for void nucleation plotted as a function of true average applied tensile stress for the various yield strength materials.

ted a strain of 0.7 before this occurs; whereas the fully aged tensile has deformed to a strain of only 0.1. The combined importance of stress and strain for the critical size particle for void initiation also exists for the Ti_2S inclusions. Since the Ti(C, N) and Ti_2S inclusion size data are similar, the Ti_2S data have been omitted for the sake of brevity. These trends which indicate the importance of stress plus strain for void formation are supported by the earlier plots in Figures 24-26 as well as the SEM fractography.

Figure 28 shows the total number of voids per unit area on the sectioning plane as a function of plastic strain for the 300 grade maraging steel at several strength levels. A void by definition consists of a voided Ti(C, N) or Ti_2S along with TiC nucleated branch cracks provided sufficient deformation has taken place for the TiC nucleated cracks to have formed. Notice that the shape of the individual curves in Figure 28 remain about the same. Early in the deformation process at all strength levels, the voids formed gradually as a function of strain. Later in the deformation process (Figure 28), the number of voids per unit area increase very rapidly. In the toughest material, the 718 MN/m^2 (104 ksi) solution treated alloy, this rapid acceleration in the number of voids does not occur until a strain of better than 1.0. The least tough 2070 MN/m^2 (300 ksi) material experiences this rapid void formation at a strain of only 0.4. The more tough the material, the more strain it will

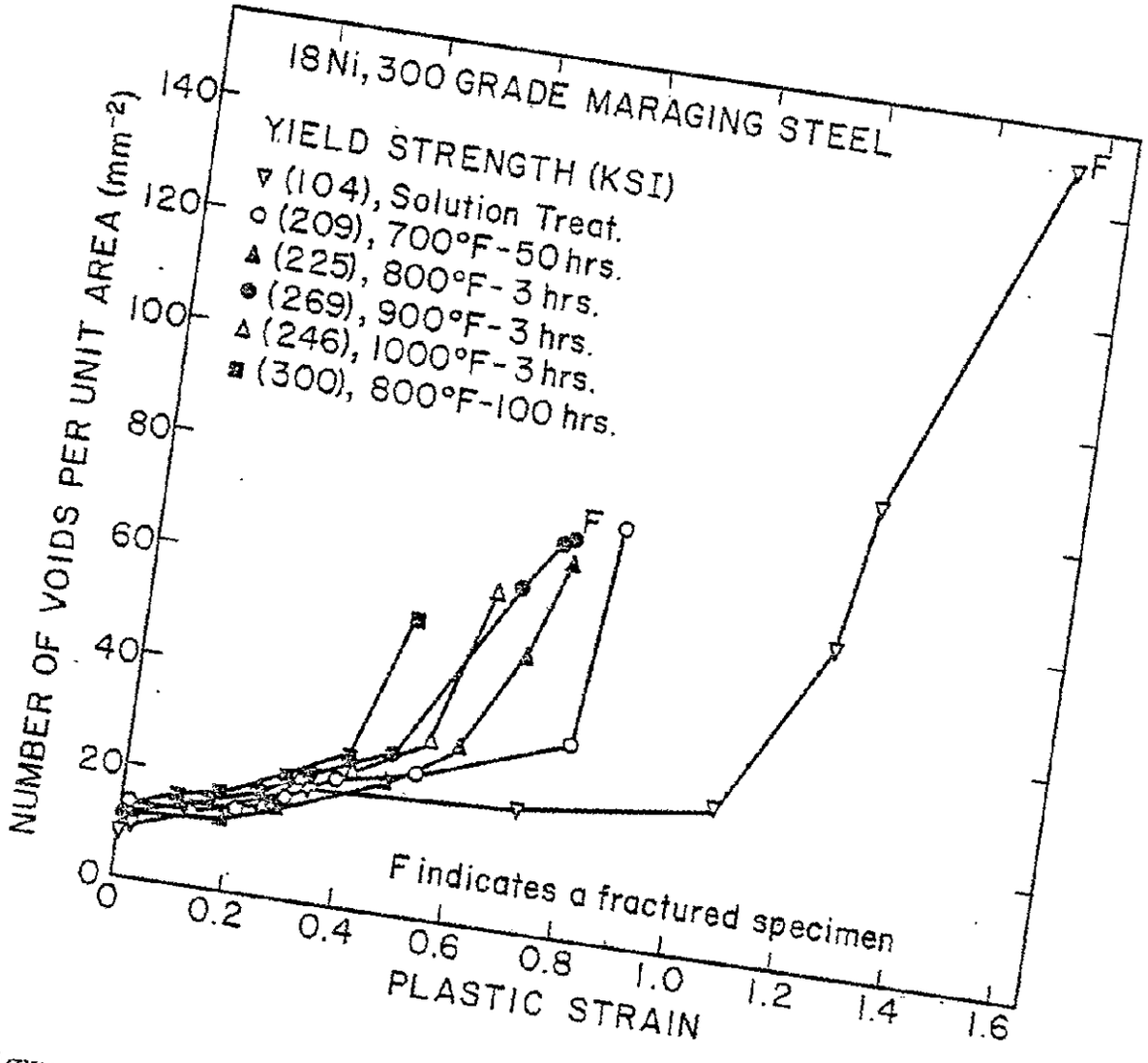

Figure 28 Variation in the number of voids per unit area plotted as a function of true plastic strain for the various yield strength materials.

tolerate and the more voids per unit area it ultimately will accommodate before failure. With increasing strength and/or overaging, toughness decreases and the amounts of stable void initiation and growth are relatively small. Since stable void nucleation and growth are prematurely terminated in the higher strength materials, many voids form, grow, and coalesce during catastrophic failure. It is for this reason, in part, that the number of measurable voids per unit area is small in the high strength conditions shown in Figure 28. The degree of stability or toughness is also indicated by the amount of TiC contribution to void growth that can be maintained and measured before instability occurs in the tensile specimen. This will be shown in the next section.

Void Growth and Coalescence

Independent of yield strength in the 300 grade alloy, the largest voids tend to grow by branching along a path of nearest neighbor critical size TiC inclusions. There is relatively little growth into the matrix by lateral growth of the original Ti(C, N) or Ti_2S inclusion nucleated void. As outlined earlier, the total void size was treated as a main void (Ti(C, N) or Ti_2S nucleated) with TiC nucleated branches. By applying the TiC branch crack shape factor determined by serial sectioning, the void areas were measured on the sectioning plane and translated to the plane of normal stress (fracture plane). The average void area was plotted as a function of true plastic strain. To pro-

perly document the relative importance of the Ti(C, N), Ti_2S, and TiC inclusion nucleated voids in the void growth process, a second graph was needed.

The progression of events leading to fracture can be followed by considering Figure 29. The average cross-sectional area of a void on the plane of normal stress experiences more rapid growth with respect to plastic strain as the material yield strength increases. The individual contributions to void growth from the Ti(C, N), Ti_2S, and TiC inclusions are shown for each yield strength in Figure 29. Note that the total amount of void growth due to the Ti(C, N) and Ti_2S inclusion nucleated voids increases continuously with strength. This is due to the rapidly increasing void nucleation rate at Ti(C, N) and Ti_2S inclusions which accompanies the increase in yield strength. This was shown earlier in Figures 24-26. The contribution to void growth from the Ti_2S inclusions is more than twice as large as the Ti(C, N) inclusion share. This is true in all yield strength materials indicated by the relative sizes of the shaded areas in Figure 29. Apparently the Ti_2S inclusion nucleated voids occupy a larger area than the Ti(C, N) inclusion nucleated voids since there are many more Ti_2S inclusions present in the material than there are Ti (C, N) particles of about the same size. Also notice from Figure 24 that in all cases a larger fraction of the Ti_2S inclusions present in the material form voids. The Ti_2S inclusions are more detrimental to ductility or toughness.

The most important change that occurs with increasing strength and/or overaging in Figure 29 is in the relative amount of TiC inclusion nucleated void area. Most of the void growth due either to the Ti(C, N) or Ti_2S inclusions occurs while the fracture process is relatively stable. Much of the unstable fracture process that takes place during the coalescence of Ti(C, N) and Ti_2S voids occurs at the TiC inclusions. For this reason, the data in Figure 29 provides an excellent measure of the relative stability of the fracture process as a function of strength. The 718 MN/m^2 (104 ksi) tensile specimen can accommodate an extensive network of TiC inclusion nucleated crack branches. In the 2070 MN/m^2 (300 ksi) material, void growth, coalescence, and fracture occurs before a total strain of 0.5. The amount of TiC nucleated voids measurable by the sectioning technique (Figure 29) markedly decreases with increasing strength and/or overaging. Because fracture surfaces from progressively stronger materials are covered by increasing amounts of TiC nucleated dimples, much of the TiC void formation must occur during the coalescence process. Void coalescence in the 1856 MN/m^2 (269 ksi) and 2070 MN/m^2 (300 ksi) materials is due in part to the termination of void growth by the rapid link-up of nearest neighbor branch cracks along voids formed at strengthening precipitates. In the overaged material, void growth is aborted at the lowest plastic strain level by rapid coalescence via the incoherent and coarsened strengthening precipitates. This explains why the lower strength overaged material can toler-

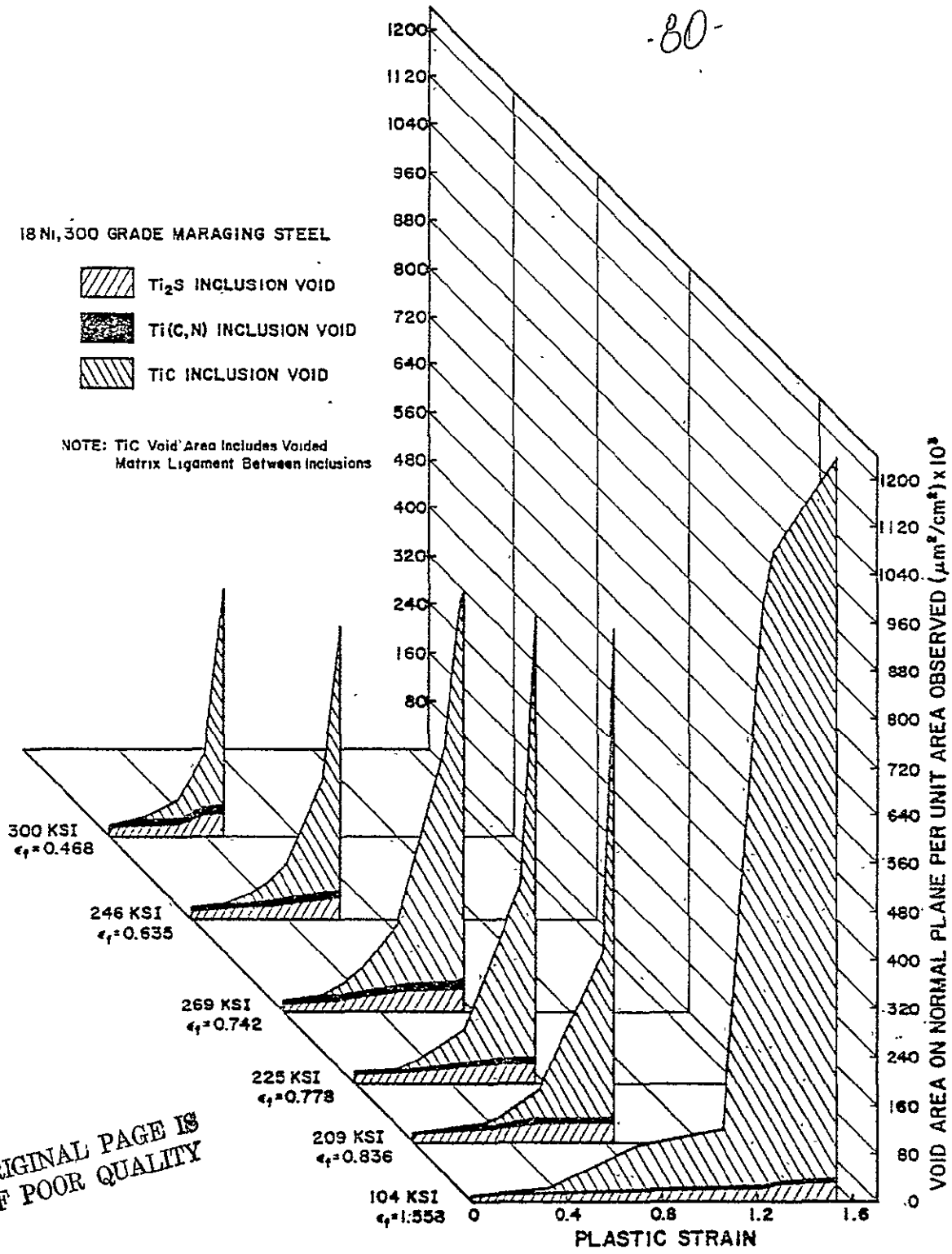

Figure 29 Individual contributions to stable void growth from the Ti(C,N), Ti_2S, and TiC inclusions plotted as a function of plastic strain for each yield strength material. The amount of stable void growth decreases in the same sequence as the loss in ductility.

ate less stable TiC nucleated void growth than the stronger, commercially aged 1856 MN/m^2 (269 ksi) material.

SUMMARY AND CONCLUSIONS

Merely satisfying the strength requirements of a particular application does not guarantee that design toughness levels will be satisfied. When dealing with most high-strength materials of a fixed composition and second-phase inclusion content (impurity level), the design engineer is faced with making a trade-off between the strength and toughness properties. An increase in the yield strength in the 18 Ni, 300 grade maraging steel from 1442 to 2070 MN/m^2 (209 to 300 ksi) can be easily attained by precipitation hardening. A significant loss in fracture toughness of from 143 to 55 MN/m^2 (130 to 50 ksi $\sqrt{in.}$) results from this difference in strengthening treatment. The goal of this research program has been to establish a microstructural basis for the decrease in toughness which results in 18 Ni, 300 grade maraging steel as strength is increased and/or the material is overaged. Once an understanding is established then a suitable means by which to control the microstructure so as to minimize the offsetting effects of these key properties might be realized.

The 18 Ni, 300 grade maraging steel is a precipitation hardenable system used here as a vehicle material with which to establish the inverse relationship between strength and toughness which is frequently observed in high-strength aluminum, titanium, and steels. A single heat of 300 grade

maraging steel has been examined throughout this study. Independent of yield strength, the material contains three types of impurity inclusions. The fixed size distributions are made up of Ti(C, N), Ti_2S, and TiC inclusions that range in size from 1 to 8 μm, 1 to 15 μm, and 0.1 to 2 μm, respectively. The variation in yield strength does result in a change in the type, size, density, and general character of the precipitate particles and the particle-matrix interface (coherency). The yield strength level establishes the relative ease with which dislocations can move in the matrix and in turn how compatible material flow is in the presence of obstructions such as impurity inclusions. At some point in the course of deformation or flow, the local restriction to flow at the inclusion can no longer be tolerated and the inclusion nucleates a void by particle cracking, particle-matrix interface decohesion, or by some mixture of both mechanisms. The energy which was stored in the particle is released and new internal surfaces are created by the formation of a void to maintain the energy balance. The matrix can then continue to flow free of this particular obstacle.

It has been found that the amount of deformation that can be accommodated by the 300 grade material without fracture sharply decreases as the yield strength is increased. The more rapid rise in stress that accompanies an equivalent increment in strain in the higher yield strength material accelerates the void initiation, growth, and coalescence processes. The initiation of voids at Ti(C, N), Ti_2S,

and TiC inclusions is not simply controlled by stress independent of strain or vice versa. A combined level of true stress and plastic strain is necessary which can be thought of as a critical energy criterion to nucleate a void at a particular size inclusion. In all yield strength marerials, the largest inclusions generally fail first in the sequence of increasing plastic strain. If an inclusion is equal to or larger than the critical size particle, then all inclusions (of the same type and character) equal to or greater than this size are likely sites for void nucleation. At an equivalent plastic strain, the critical size inclusion for void formation decreases with increasing matrix yield strength. From plots of inclusion diameter (Ti(C, N) or Ti_2S) versus true tensile stress, Bridgman corrected stress, true plastic strain, and several other variations, it has been concluded that the critical size inclusion criterion is not dependent upon any single variable. Void initiation is apparently most dependent on, but in no way entirely controlled by, the stress level. The critical size criterion is some complex function of stress and strain, particle type, yield strength, particle hardness relative to the matrix, and integrity of the particle-matrix bond. Observations of void nucleation at Ti(C, N) and Ti_2S inclusions at several stress, strain, and yield strength combinations have shown that the critical size for particle failure is in some way qualitatively related to the energy or work (product of stress and strain) put into the system.

As deformation proceeds, the Ti(C, N) and Ti_2S inclusions serve to obstruct the flow of the matrix. In higher strength materials, the amount of plastic strain that can be accommodated before void initiation is suppressed due to more rapid rise in tensile stress. As adequate levels of stress and strain are attained, additional voids nucleate while previously nucleated voids continue to grow. The Ti(C, N) and Ti_2S inclusions fail by a combination of particle cracking and particle-matrix interface decohesion. The overall rate of void nucleation is accelerated in direct relation to increasing yield strength. Void nucleation at Ti(C, N) and Ti_2S inclusions in the overaged material occurs at a frequency similar to void nucleation in underaged material of equivalent yield strength. Note that this is not the case for void coalescence since precipitates are activated in the overaged condition leading to premature termination of void growth.

The voids formed at the Ti(C, N) and Ti_2S inclusions grow by a combination of limited longitudinal elongation of the main void along the tensile axis and primarily by lateral crack branching along a path of TiC inclusion nucleated voids. The TiC inclusion nucleated crack progresses by a repetitive process of void nucleation at a TiC particle followed by matrix tearing to the next TiC inclusion, etc. The process of void growth occurs more rapidly as a function of plastic strain with increasing material yield strength. The total number of voids nucle-

ated increases significantly as the yield strength increases. As such, the amount of void growth necessary for nearest neighbor voids to impinge is greatly reduced. The lowest strength materials can tolerate the largest voids without fracture. The total area of stable void growth by TiC inclusion nucleated voids along crack branches is sharply reduced as the strength is increased or the material is overaged. Large voids become unstable and lead to coalescence by impingement of adjacent TiC nucleated branches in the low strength materials. In all cases, the TiC inclusions nucleate voids by particle-matrix failure.

Coalescence of the branched voids occurs in the three highest strength materials by a combination of cracking along TiC inclusions and by premature separation at Ni_3Mo or Fe_2Mo precipitates along intense shear bands in the matrix ligaments between TiC nucleated branch cracks. The combination of shear stresses and precipitate size are sufficient to activate voids during unstable fracture in the three strongest materials. The void nucleation at strengthening precipitates serves to abort the stable void growth process. The 2070 MN/m^2 (300 ksi) material accommodates the least amount of stable TiC nucleated void growth, activates precipitates as void sites at the lowest plastic strain, and in turn results in the lowest ductility or toughness. This condition represents the maximum room temperature yield strength that is attainable in this heat of 300 grade maraging steel.

These findings are complemented by the fractographic information taken from both tensile and K_{Ic} fracture surfaces. The number of dimples per unit area of fracture surface increases with increasing yield strength in direct proportion to the void nucleation rate. The average dimple size decreases continuously with increasing strength and/or overaging which follows directly from the decreasing amount of stable void growth measured by sectioning tensile specimens. More than half of the fracture surface at all strength levels is covered by 2-3 μm diameter TiC nucleated dimples. The interparticle spacing between TiC inclusions in the matrix is about 2-3 μm which clearly explains the separation or dimple size on the fracture surface. The precipitate nucleated dimples (when present) are of a submicron size which relates to the size and spacing between strengthening precipitates. The areal fraction of precipitate nucleated dimples is largest in the overaged tensile or K_{Ic} fractures, since there the precipitates are now larger and less coherent with the matrix than in any other condition considered. In this strength level, many of the coarse (500-1000 Å) precipitates are now likely sites for void formation even though the yield strength has decreased significantly from the fully aged material. This explains why the overaged material at a yield strength of 1697 MN/m^2 (246 ksi) is much less tough than an equivalent yield strength underaged material. The 2070 MN/m^2 (300 ksi) tensile specimen fracture contains the next largest amount of preci-

pitate nucleated dimples. The 2070 MN/m^2 (300 ksi) tensile fracture contains the largest total number of dimples per unit area and likewise the smallest dimples. This fractographic observation is consistent with the sectioned tensile data in explaining why the fully strengthened material is the least tough alloy.

With the combined sectioned tensile and fractographic techniques, a better understanding of the effect of material strength on the void initiation growth and coalescence process of fracture has been reached. By establishing the influence of deformation, as measured by stress and strain, on the inclusions and strengthening precipitates which serve as restrictions to flow, a better understanding of the inverse trend between strength and toughness has been accomplished.

Void nucleation at any strength level is largely controlled by the number, size, shape, and integrity of the Ti(C, N) and Ti_2S inclusions. Significant improvement in the toughness of the 300 grade maraging steel at any yield strength can be realized if lower carbon, sulfur, and nitrogen levels are maintained. There are also several ways of improving the toughness by manipulating the material with altering the purity which should be considered.

As the 300 grade maraging steel is made stronger by the degree to which it is age hardened, the localized stresses and strains will be fixed by the yield strength of flow properties. Without significant changes in the alloy composition, the fracture toughness of the 300 grade

maraging steel can be increased at all strength levels by decreasing the size and volume fraction of Ti(C, N) and Ti_2S inclusions. This can be accomplished by improved melting practice and cleaner starting materials. Another approach can utilize ways of increasing the nucleation sites in the molten metal for the formation of Ti(C, N) and Ti_2S inclusions. Small amounts of zirconium have been isolated in the centers of many Ti(C, N) inclusions. This material evidently has a higher melting point than the Ti(C, N) inclusion and thus serves as an excellent nucleation site at which the inclusion can form as the liquid metal is cooled. Investigation of techniques by which to seed the metal during deoxidation practice could serve as an effective way of increasing the number of inclusions at a fixed volume fraction of impurity. This would reduce the size of the average Ti(C, N) or any other inclusion so as to make subsequent void nucleation more difficult. Finer Ti(C, N) and/or Ti_2S inclusions should serve to delay void initiation to higher stresses and thus higher yield strength can be utilized without as significant a loss in fracture toughness. Any stirring action that can homogeneously distribute the inclusions throughout the melt will reduce the tendency of these inclusions to cluster and serve to maximize the interparticle spacing and void growth distances. In materials where inclusions are highly clustered, the effective inclsuion diameter is the sum of the individual particle diameters in the cluster. A very large void is opened up

as soon as the individual particles fail since virtually no void growth can take place before nearest neighbor impingement.

Elimination or reduction in the size and volume fraction of the TiC inclusions represents another approach to minimize the K_{Ic} decrease with increasing yield strength. The total volume fraction of inclusions in this material amounted to better than 1.3 volume percent. This consisted primarily of the TiC inclusions which made for a volume fraction of about 1.0%. This resulted in a material which was no better than average with respect to cleanliness. Based upon the particularly large number of TiC inclusions and the extremely important role played by these inclusions, work on controlling these particles is suggested. By reducing the tendency for voids to form at TiC inclusions, the amount of stable void growth at the Ti(C, N) and Ti_2S sites would increase. The TiC inclusions are formed in the solid state while the material is in the austenitic condition. Critical examination of the cooling cycle through the 870 to 1093°C (1600 to 2000°F) temperature range is necessary. A careful hot working procedure could potentially leave the Ti(C, N) and Ti_2S inclusions free of any cracks or voids prior to deformation of the tensile or K_{Ic} specimens. This would also serve very effectively in producing a much tougher starting material. To combat the high affinity of titanium for carbon and sulfur, it is suggested that subsequent experimental heats be made with as low a titanium addition as possible and still get

the required yield strength. This may require alloy development work aimed at varying the relative amounts of nickel, cobalt, molybdenum, and titanium to arrive at a material with better inclusion control.

The void coalescence process can be delayed by eliminating or, at least, altering the size distribution of TiC inclusions. In addition, work aimed at controlling the number, size, and coherency of strengthening precipitates would simultaneously benefit the strength and toughness properties. If the precipitates would be maintained as extremely small (less than 200 Å) and coherent particles, fracture toughness might be extended without sacrificing as much yield strength. Additional work to understand the role of cobalt in promoting planar slip in the maraging steel would benefit the entire program. If slip could be made less planar, it is conceivable that the intensity of localized shear bands could be reduced and in turn void coalescence at precipitates delayed or even eliminated.

It is very important to remember that these techniques that have been suggested will apply to any other high-strength alloy system. The processes of void initiation, growth, and coalescence are dependent upon the inclusions and the particular alloy system in which they exist. In all cases, if adequate amounts of stress and strain are coupled with second-phase particles of sufficient size and other characteristics, then void nucleation will most likely occur. The size, shape, volume fraction, and interparticle spacing are among the key design options in con-

trolling the properties of alloys and, in particular, the maximum simultaneous strength-toughness that is attainable.

REFERENCES

1. J. R. Low, Jr., Prog. Mat. Sci., 12 (1) (1963) p. 4.

2. D. Broek, "A Study on Ductile Fracture," Ph.D. Thesis, Delft Technological University (1970).

3. T. B. Cox and J. R. Low, Jr., Met. Trans., 5 (1974) pp. 1457-1470.

4. R. H. Van Stone and T. B. Cox, ASTM STP 600 (1976) p. 5.

5. S. Floreen, "The Physical Metallurgy of Maraging Steels," in: Metallurgical Reviews, 126 (1968) p. 115.

6. D. T. Peters, Trans. ASM, 61 (1968) p. 62.

7. J. M. Chilton and C. J. Barton, Trans. Quart. ASM, 60 (1967) p. 528.

8. H. J. Rack and D. Kalish, Met. Trans., 2 (1971) p. 3011.

9. W. A. Spitzig, J. M. Chilton, and C. J. Barton, Trans. ASM, 61 (1968) p. 635.

10. "Standard Method of Test for Plane-Strain Fracture Toughness of Metallic Materials," ASTM Designation E399-74, ASTM Standards, Part 31 (1974).

11. T. Boniszewski and E. Boniszewski, JISI, 204 (1966) p. 360.

12. E. Nes and G. Thomas, Met. Trans., 7A (1976) p. 967.

13. F. C. Hull and W. J. Houk, Trans. AIME, 197 (1953) p. 565.

14. E. J. Meyers, Proc. First Int. Cong. Stereology, Vienna (1963) p. 151.

15. R. T. DeHoff and F. N. Rhines, Trans. AIME, 221 (1961) p. 975.

16. R. T. DeHoff, "Measurement of Number and Average Size in Volume," in Quantitative Microscopy, eds. R. T. DeHoff and F. N. Rhines, McGraw-Hill, New York (1968) p. 128.

17. T. J. Koppenaal, "Dynamic Fracture Toughness Measurements Using Precracked Charpy Samples," Aeronutronic Division of Philco-Ford Corp., Newport Beach, California (1973).

18. M. H. Jones and W. F. Brown, Jr., Review of Developments in Plane Strain Fracture Toughness Testing, ASTM STP 463 (1970) p. 63.

19. J. A. Psioda, "The Effect of Microstructure and Strength on the Fracture Toughness of an 18 Ni, 300 Grade Maraging Steel," Ph.D. Thesis, Carnegie-Mellon University, 1977.

20. R. H. Van Stone, R. H. Merchant, and J. R. Low, Jr., ASTM STP 556 (1973) p. 93.

21. D. P. Clausing, "Comparison of Plane Strain and Axisymmetric Plastic Flow and Fracture," U. S. Steel Technical Report 36.006-001(2), August 1972.